Loss of Oxidation Resistance 1, *OXR1*, Is Associated with an Autosomal-Recessive Neurological Disease with Cerebellar Atrophy and Lysosomal Dysfunction

Julia Wang,[1,2] Justine Rousseau,[3] Emily Kim,[4] Sophie Ehresmann,[3] Yi-Ting Cheng,[5] Lita Duraine,[2,6] Zhongyuan Zuo,[2,6] Ye-Jin Park,[2,6] David Li-Kroeger,[2,6] Weimin Bi,[6] Lee-Jun Wong,[6] Jill Rosenfeld,[6] Joseph Gleeson,[7] Eissa Faqeih,[8] Fowzan S. Alkuraya,[9] Klaas J. Wierenga,[10,11] Jiani Chen,[10,12] Alexandra Afenjar,[13,14] Caroline Nava,[13] Diane Doummar,[15] Boris Keren,[13] Jane Juusola,[16] Markus Grompe,[17,18] Hugo J. Bellen,[2,5,6,19,*] and Philippe M. Campeau[3,*]

We report an early-onset autosomal-recessive neurological disease with cerebellar atrophy and lysosomal dysfunction. We identified bi-allelic loss-of-function (LoF) variants in Oxidative Resistance 1 *(OXR1)* in five individuals from three families; these individuals presented with a history of severe global developmental delay, current intellectual disability, language delay, cerebellar atrophy, and seizures. While *OXR1* is known to play a role in oxidative stress resistance, its molecular functions are not well established. OXR1 contains three conserved domains: LysM, GRAM, and TLDc. The gene encodes at least six transcripts, including some that only consist of the C-terminal TLDc domain. We utilized *Drosophila* to assess the phenotypes associated with loss of *mustard (mtd)*, the fly homolog of *OXR1*. Strong LoF mutants exhibit late pupal lethality or pupal eclosion defects. Interestingly, although *mtd* encodes 26 transcripts, severe LoF and null mutations can be rescued by a single short human *OXR1* cDNA that only contains the TLDc domain. Similar rescue is observed with the TLDc domain of *NCOA7*, another human homolog of *mtd*. Loss of *mtd* in neurons leads to massive cell loss, early death, and an accumulation of aberrant lysosomal structures, similar to what we observe in fibroblasts of affected individuals. Our data indicate that *mtd* and *OXR1* are required for proper lysosomal function; this is consistent with observations that *NCOA7* is required for lysosomal acidification.

Introduction

Oxidation Resistance 1 (*OXR1*) (HGNC: 15822, MIM: 605609) was first identified based on its ability, when overexpressed, to reduce DNA lesions induced by oxidative stress in *E. coli*.[1,2] In an SOD1^{G93A} ALS (amyotrophic lateral sclerosis [MIM: 105400]) mouse model, overexpression of OXR1 was shown to delay the onset of symptoms.[3,4] Other functions associated with OXR1 include neuronal maintenance,[3–6] mitochondrial morphology and DNA maintenance,[7–9] regulation of aging,[10,11] innate immune defense,[12–14] protection against Lupus nephritis (MIM: 601744),[15] regulation of the cell cycle,[9,16] and modulation of glycolytic pathways.[17] While these studies have shown that OXR1 may affect several cellular processes, its mechanism of action is still ill defined, and the gene has not been previously associated with a human disease.

OXR1 has a complex gene structure. Six validated isoforms ranging from 216 to 874 amino acids in length are reported in RefSeq. The longest isoform has three protein domains: LysM, GRAM, and TLDc.[18] LysM (lysin motif) is a globular domain of 42 amino acids.[18] It is involved in binding peptidoglycan in bacteria and chitin in eukaryotes, but proteins involved in several other biological functions also contain this domain.[19] The GRAM (glucosyltransferases, Rab-like GTPase activators and myotubularins) domain has a structure similar to those of Pleckstrin homology (PH) domains, it consists of about 70 amino acids[18] and it is most likely a lipid-binding signaling or intracellular protein-binding domain important for membrane-associated processes.[19] The TLDc (TBC [Tre-2/Bub2/Cdc16] and LysM domain containing protein) domain has low structural similarity to known domains[20] and is 136 amino acids in length.[18] Previous

[1]Program in Developmental Biology, Medical Scientist Training Program, Baylor College of Medicine, Houston, TX 77030, USA; [2]Jan and Dan Duncan Neurological Research Institute, Baylor College of Medicine, Houston, TX 77030, USA; [3]Centre Hospitalier Universitaire Saint-Justine Research Center, CHU Sainte-Justine, Montreal, QC H3T 1J4, Canada; [4]Biochemistry and Cell Biology, Rice University, Houston, TX 77005, USA; [5]Program in Developmental Biology, Baylor College of Medicine, Houston, TX 77030, USA; [6]Department of Molecular and Human Genetics, Baylor College of Medicine, Houston, TX 77030, USA; [7]Rady Institute of Genomic Medicine, University of California San Diego, La Jolla, CA 92093, USA; [8]Section of Medical Genetics, Children's Hospital, King Fahad Medical City, Riyadh, 11525, Saudi Arabia; [9]Department of Genetics, King Faisal Specialist Hospital and Research Center, Riyadh, 11525, Saudi Arabia; [10]Department of Pediatrics, Oklahoma University Health Sciences Center (OUHSC), Oklahoma City, OK 26901, USA; [11]Department of Clinical Genomics, Mayo Clinic Florida, Jacksonville, FL 32224, USA; [12]Division of Genomic Diagnostics, Children's Hospital of Philadelphia, Philadelphia, PA 19104, USA; [13]Assistance Publique des Hôpitaux de Paris, Unité de Génétique Clinique, Hôpital Armand Trousseau, Groupe Hospitalier Universitaire Paris, 75012, France; [14]Département de Génétique et Embryologie Médicale, CRMR des Malformations et Maladies Congénitales du Cervelet, GRC ConCer-LD, Sorbonne Universités, Hôpital Trousseau, Paris, 75012 France; [15]Assistance Publique des Hôpitaux de Paris, Service de Neuropédiatrie, Hôpital Armand Trousseau, Groupe Hospitalier Universitaire Paris, 75012 France; [16]GeneDx, Inc., Gaithersburg, MD 20877, USA; [17]Department of Pediatrics, Oregon Health and Science University, Portland, Oregon 97201, USA; [18]Department of Molecular and Medical Genetics, Oregon Health and Science University, Portland, Oregon 97201, USA; [19]Howard Hughes Medical Institute and Department of Neuroscience, Baylor College of Medicine, Houston, TX 77030, USA

*Correspondence: hbellen@bcm.edu (H.J.B.), p.campeau@umontreal.ca (P.M.C.)

https://doi.org/10.1016/j.ajhg.2019.11.002.

studies, however, have not reached a consensus on the function of the TLDc domain.[21,22]

In the current study, we report five individuals, from three families, with bi-allelic loss-of-function (LoF) variants in *OXR1*. Individuals with *OXR1* deficiency have cerebellar atrophy, developmental delay, and other phenotypes. We generated a fly model of *OXR1* deficiency in which the fly gene *mustard* (*mtd)* can be functionally replaced by a short human *OXR1* or *NCOA7* (HGNC: 21081, MIM: 609752) cDNA. *mtd* mutant flies have severe neurological defects but experience unexpectedly low oxidative stress. Finally, using transmission electron microscopy (TEM), we examined the sub-cellular structures in *OXR1/mtd*-deficient fly neurons and human fibroblasts, and we found a predominant lysosomal dysfunction with a concomitant accumulation of aberrant lysosomal structures.

Material and Methods

Human Genetics

For family 1, trio exome sequencing and analysis was conducted at GeneDx.[23] Assertion criteria for variant classification are available at ClinVar. For families 2 and 3, exome sequencing and analysis were performed as previously described (family 2[24] and family 3[25]). The cohort was assembled using GeneMatcher[26] for Individuals 1 and 2 and by discussion between collaborators for family 3. *OXR1* variants are mapped onto transcript at RefSeq accession number NM_018002.3 (RefSeq NP_060472.2). This study was approved by the local institutional review board (IRB), and appropriate informed consent was obtained from human subjects. Centre Hospitalier Universitaire (CHU) Sainte-Justine Federalwide Assurance (FWA) number IRB00002927, Protocol number 4181.

Sanger Sequencing

Sequence alignment and figures were done using the bioinformatics software Geneious from Biomatters.

Cell Culture

Primary human fibroblast cell lines were generated from skin biopsy according to an established protocol[27] and maintained in DMEM supplemented with 15% fetal bovine serum (FBS) and antibiotics. All experiments were conducted with cell lines below passage number ten.

LysoTracker Staining

Fibroblasts were seeded in a Lab-Tek Chambered Coverglass system one day before the experiment. LysoTracker Red (L7528) stock (1mM) from Invitrogen was diluted at 1:2000, and Hoechst was diluted at 1:1000 in cell culture media and incubated with the cells for 30 min at 37°C and then washed with media and immediately imaged live for at least 10 fields from three biological replicates per group. All images were taken with the same microscope settings. Each image was taken at the Z position, where the nuclei (Hoechst staining) are at their maximum size. LysoTracker stainings of fibroblasts were quantified by number of LysoTracker punctae in each field divided by number of nuclei.

Propidium Iodide and Hoechst Staining

Fibroblasts were seeded in a Lab-Tek Chambered Coverglass system at 40% confluence one day before the experiment. Cells were treated with serum-free cell culture media with or without 500μM H_2O_2 for 4 h. Propidium iodide (PI, ThermoFisher P1304MP, 1 mg/mL stock solution) and Hoechst 33342 (ThermoFisher H3570) were diluted 1,000× in cell culture media.[28] Cells were washed twice with PBS after H_2O_2 treatment and incubated with diluted PI and Hoechst 33342 for 15 min. They were then washed twice with PBS. Fresh media was added, and the cells were immediately imaged live from three biological replicates for at least five fields per group. All images were taken with the same microscope settings (Hoechst 33342: 350/461 and PI: 535/617).

mtDNA Long Read Sequencing

10 cm plates of 80% confluent fibroblasts from Individual 2 with or without 1 h exposure to 0.75mM H_2O_2 were collected.[9] Total DNA from fibroblast samples was isolated with PureLink Genomic DNA Mini Kit (ThermoFisher). mtDNA was amplified with long-range PCR and run on HiSeq2000 with MiSeq Reagent Kit v3 (Illumina, MS-102-3001).[29,30]

Fly Strains and Assays

Flies were raised at 22°C under standard conditions unless stated otherwise. Fly strains used are listed in Table S1.

Lifespan assays were conducted with 15–20 flies per vial, transferred every 2 days, and flies were counted every day; at least 100 flies from three independent crosses were assayed for each genotype.

Climbing assays were conducted by collecting progeny from three independent crosses for each genotype. The flies were aged for 2–3 days. Flies were then transferred from standard food vials to an empty vial marked at 15 cm from the bottom. Flies were knocked down to the bottom of the vial by tapping the vial. Flies were allowed 20 s to climb past the 15 cm mark, and least 10 vials with 10 flies per vial were tested. The percentage of flies able to climb past 15 cm was determined, the test was conducted in triplicate, and this result was indicated by a single data point. At least 100 flies were tested for each genotype.

Bang sensitivity assays were conducted by collecting progeny from three independent crosses for each genotype. The flies were aged for 2–3 days. At least 10 vials with 10 flies per vial of the same genotype were transferred from standard food vials to an empty vial and vortexed for 10 s.[31] The flies were allowed 30 s to stand upright. Flies that remained on their backs or sides were recorded as failure to stand up. Each data point represents 10 flies, and at least 100 flies were tested for each genotype.

For the *in vivo* redox indicator assays, adult mutant (*mtd-t2a-gal4/Df(3R)3-4*) or control (*mtd-t2a-gal4/+*) flies with redox indicators between day 1 and 2 were anesthetized and rinsed in 70% ethanol. They were transferred onto a dissection pad and fixed with a needle, and the brains were dissected. Three calibration samples were dissected in PBS, treated with either 20mM DTT (dithiothreitol) or 2mM DA (diamide) for 10 min, and blocked with NEM (N-ethyl maleimide) for 10 min. All other sample dissections were performed in 20mM NEM. All samples were further incubated with NEM for 10 min at room temperature (RT) after dissection. NEM was removed by rinsing once with PBS. Then samples were fixed with 4% PFA for 1 h at RT on a shaker. PFA was removed by washing twice with PBS for 10 min. Samples

were placed under vacuum for 10 min six times, and samples were mounted onto glass slides with VectaShield. Probe fluorescence was excited sequentially at 405 and 488 nm (line by line) and detected at 500–530 nm on a Leica SP8 confocal microscope. All images were taken with the same microscope settings. Images were analyzed with ImageJ and processed by taking the maximum intensity for the z stacks of both channels, correcting background with rolling ball, adjusting image to 32-bit, selecting the 488 nm (green) image to threshold, and measuring the ratio of 405nm/488nm.[32]

For the aconitase enzymatic activity assay, three biological replicates for each group were tested. Ten adult fly heads of elav > *luciferase* RNAi or elav > *mtd* RNAi at day 5 were homogenized for each sample, and subsequent steps used the reagents and protocol from BioVision Aconitase Activity Colorimetric Assay Kit (#K716-100).[33]

For antioxidants and oxidants drug feeding, 1 day old elav > *mtd* RNAi flies were put on regular food mixed with drugs at the following concentrations: DMSO (0.1%, Sigma 276855), NAC (500μM, Sigma A7250), Oltipraz (1mM, Sigma O9389), tBHQ (6mM, Sigma 112941), D3T (2mM, Abcam ab141925), and Rotenone (100μM, Sigma R8875).[34–37] Flies were transferred to new food every 3 days and counted every day for more than 100 flies per group. Flies from each experiment were obtained from three independent crosses. Due to rotenone's light sensitivity, flies fed with Rotenone were raised in constant darkness in 25°C. For feeding with H_2O_2 (5% or 15% in 5% Sucrose), vials were loaded with two pieces of Whatman filter paper holding 400 μL of 5% sucrose solution alone (controls) or 400 μL of 5% sucrose solution with 5% or 15% (v/v) H_2O_2.[38] At least 10 vials with 10 flies per vial of each genotype were raised at 25°C, and the flies were transferred to new vials every other day with fresh filter paper with the respective treatment. The vials were topped up with 300 μL 5% sucrose on the days between vial changes.[38] Dead flies in each vial were scored daily.

For Acridine Orange (AO) staining, 1.3 μL of 1mM AO (Invitrogen, A1301) was diluted in 1 mL of PBS.

On days 3 and 6, Elav > *luciferase* RNAi or Elav > *mtd* RNAi fly brains were dissected in PBS, washed with PBS, and then incubated in 150 μL AO for 10 min. The tissue was washed three times with PBS, mounted in VectaShield, and imaged immediately under the same conditions and confocal microscope settings with excitation at 561 nm and emission at 579–620 nm.[39,40] The images were analyzed by summing the slices and measuring the mean gray intensity of the fly brain.

Immunoblot and Immunostaining

Antibodies used for immunoblot are: rabbit anti-OXR1 (Bethyl A302-035A, 1:500 dilution), rabbit anti-OXR1 (Sigma HPA027395, 1:500), rabbit anti-GAPDH (Cell Signaling,14C10, 1:10,000 dilution), mouse anti-LAMP2 (Santa Cruz Biotech, sc-18822, H4B4, 1:1000 dilution), anti-rabbit HRP secondary (Jackson ImmunoResearch, 323-005-021, 1:10,000 dilution), and anti-mouse HRP secondary (Jackson ImmunoResearch, 115-035-003, 1:10,000 dilution). All antibodies were diluted in 5% nonfat milk or 5% BSA in TBS-T. Each fibroblast immunoblot was repeated with three biological replicates.

For immunostaining of fibroblasts, the following antibodies were used: rabbit anti-RAB7A (Rab7) (Cell Signaling, D95F2, 1:100), DAPI, and donkey anti-rabbit Alexa 647 conj. (Jackson ImmunoResearch, 1:500). Each datapoint is the number of puncta divided by number of nuclei in one field of view. All experiments, including three biological replicates, were imaged with the same microscope settings.

Antibodies used for fly head immunoblots were: rabbit anti-Ref(2)p (gift from Dr. Sheng Zhang[41]) and anti-rabbit HRP secondary (Jackson ImmunoResearch, 323-005-021, 1:10,000 dilution).

Antibodies used for fly brain immunostaining were: mouse anti-Prospero (DSHB, MR1A, 1:20[42]), mouse anti-CHP (Chaoptin) (DSHB, 24B10, 1:20[43]), rat anti-HA (Roche, 3F10, 1:50), donkey anti-mouse Alexa 647 conj. (Jackson ImmunoResearch, 1:500), and donkey anti-rat Alexa 488 conj. (Jackson ImmunoResearch, 1:500).

Hematoxylin and Eosin (H&E) Staining

For histology, fly heads were fixed in 8% glutaraldehyde for 4 days and embedded in paraffin. Tangential (3 μm) retinal sections were cut using a Leica Microtome (RM2245) and stained with hematoxylin and eosin. All experiments were processed and stained with the same conditions and imaged with the same microscope settings.

Transmission Electron Microscopy

Drosophila retina ultrastructure was imaged following standard electron microscopy procedures and using a Ted Pella Bio Wave processing microwave with vacuum attachments.[44,45] In brief, whole heads were dissected in order to preserve the brain tissue. The tissue was covered in 2% paraformaldehyde, 2.5% glutaraldehyde, in 0.1 M sodium cacodylate buffer at pH 7.2. After dissection, the heads were incubated overnight for up to 3 days in the fixative on a rotator. The pre-fixed heads were then fixed again, rinsed 3× with millipore water, post-fixed with 1% aqueous osmium tetroxide, and rinsed again 3× with millipore water. Ethanol concentrations from 25%–100% were used for the initial dehydration series, followed with propylene oxide as the final dehydrant. Samples were gradually infiltrated with three ratios of propylene oxide and Embed 812, finally going into three changes of pure resin under vacuum. Samples were allowed to infiltrate in pure resin overnight on a rotator. The samples were embedded into flat silicone molds and cured in the oven at 62°C for 3 days. The polymerized samples were thin-sectioned at 48–50 nm and stained with 1% uranyl acetate for 10 min, then stained with 2.5% lead citrate for two min before they were examined via TEM. Grids were viewed in a JEOL JEM 1010 transmission electron microscope at 80kV. Images were captured using an AMT XR-16 mid-mount 16-megapixel digital camera. All experiments were processed and stained with the same conditions and imaged with the same microscope settings.

Statistical Methods

Two-tailed Student's t tests were conducted for data unless otherwise specified. ns indicates p value > 0.05, * indicates p value ≤ 0.05, ** indicates p value ≤ 0.01, *** indicates p value ≤ 0.001, and **** indicates p value ≤ 0.0001. Error bars represent the standard error of the mean.

Results

Description of Clinical Phenotypes in Affected Individuals

Five affected individuals from three families (Figure 1A) presented with a history of past severe global

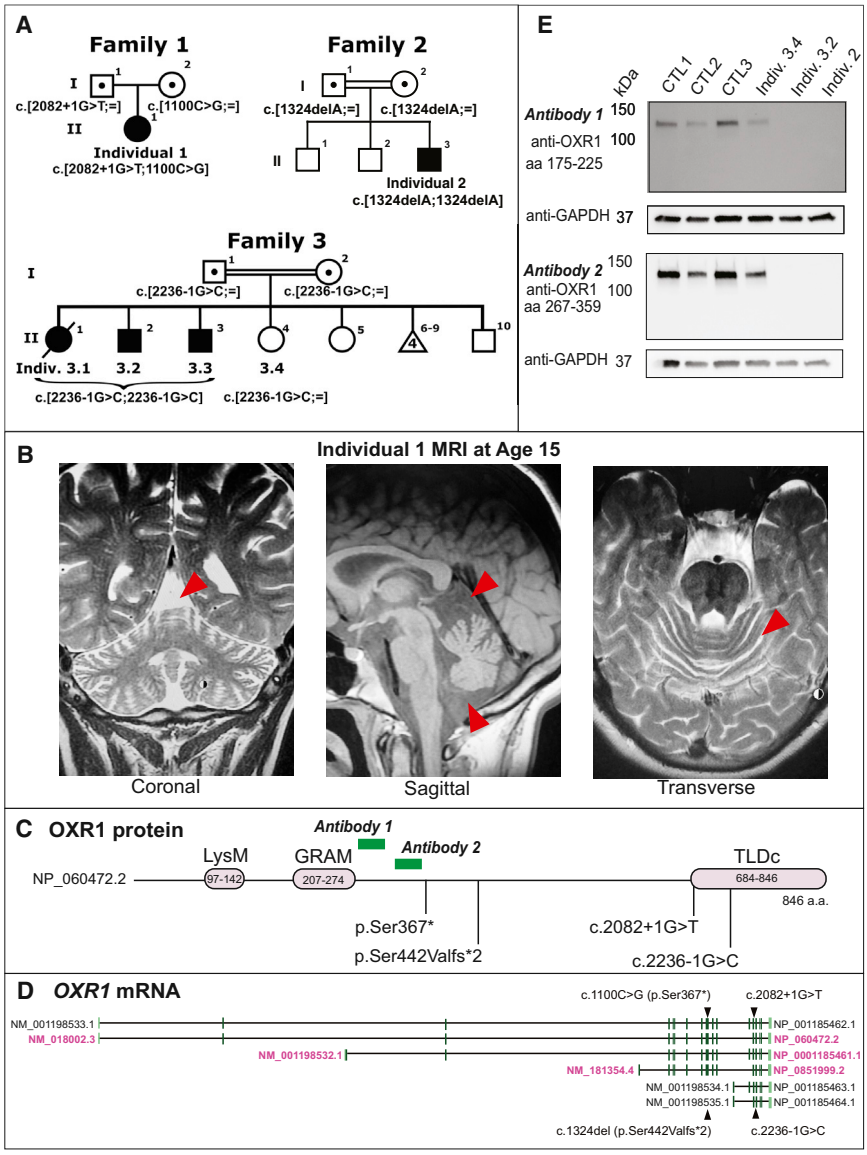

Figure 1. Five Affected Individuals Have Bi-Allelic Loss-of-Function Variants in *OXR1*

(A) Pedigrees from three families show affected individuals and the *OXR1* variants inherited. In Family 1, the parents are each carriers for a single copy of a different variant (one splice site and one nonsense variant) in *OXR1,* and they have one affected daughter who inherited both variants. In Family 2, the parents are consanguineous and are carriers of the same variant. Family 2 has two unaffected males and one affected male, indicated as Individual 2. In Family 3, the parents are also consanguineous and are carriers of the same variant. Family 3 has one affected female (Individual 3.1) and two affected males (Individuals 3.2 and 3.3). Individual 3.4 is an unaffected female sibling who is a carrier of the variant.

(B) Magnetic resonance imaging (MRI) images from Individual 1 when she was 15 years old. Three perspectives are shown (from left to right): coronal, sagittal, and transverse. On coronal and sagittal views, we note the marked cerebellar atrophy as can be evidenced by the increased cerebrospinal fluid space above and below the cerebellum (arrowheads), and the prominent cerebellar folia. On the transverse view, we see wide cerebellar fissures.

(C) *OXR1* encodes a protein with 846 amino acids (RefSeq NM_018002.3). It has three protein domains: LysM (aa 97 to 142), GRAM (aa 207 to 274), and TLDc (aa 684 to 846). The four variants found in affected individuals are mapped to their locations on the protein. The green bars indicate the antigens that the two antibodies used in Figure 1D immunoblots were raised against.

(D) *OXR1* has six validated RefSeq mRNA transcripts. Three transcripts (in black) are not expressed in the central nervous system (CNS), and the other three transcripts (in magenta) are expressed in the CNS. Each of the *OXR1* variants is mapped onto the transcripts where all three transcripts that are expressed in the CNS contain all four variants. The protein of the second variant, RefSeq NM_0.18002.3 or RefSeq NP_060472.2, is shown in Figure 1D.

(E) Two antibodies were used to detect OXR1 protein levels in fibroblasts from four control individuals, including an unaffected sibling from Family 3. The antibodies used are: Bethyl A302-035A (epitope 175- 225) and Sigma HPA027395 (epitope 267- 359). GAPDH is used as loading control. No truncated proteins can be detected on immunoblots with either antibody. At least three biological replicates were tested, and representative images are shown.

developmental delay as well as current intellectual disability, cerebellar atrophy, hypotonia, language delay, and seizures (Table 1). Four individuals are currently between the ages of 12 and 20, and one individual died at age 11. Each individual is described in detail below, and their symptoms are summarized in Table 1.

Individual 1 is a 20-year-old female with previous developmental delay, current intellectual disability, epilepsy, and scoliosis. She was first evaluated by her geneticist at age 13. At that time, her weight and height were at 0.1 percentile for her age. She was not toilet trained for either bowel or urinary system, and she was non-verbal. She was able to walk without help and had no structural malformations. Developmental delay and hypotonia were first observed at about 6–7 months of age, and she continued to have global developmental delay without regression; this delay evolved into intellectual disability. She developed seizures at age 10. Imaging revealed a 48–49 degree right thoracic scoliotic curve when she was 13; she later had surgical repair for this. She had delayed puberty and delayed bone age without known causes. At age 15, her brain MRI showed cerebellum volume loss and prominent cerebellar folia (Figure 1B). At age 17, she displayed severe intellectual disability and her seizures were mostly under control by medication. Her height was at the 23rd percentile for her age and her weight was at the 8th percentile.

Table 1. Summary of Clinical Phenotypes Observed in Cases 1, 2, and 3.1–3.3

	Family 1	Family 2	Family 3		
Individual	**1**	**2**	**3.1**	**3.2**	**3.3**
Current age (year)	20	12	deceased at age 11	15	13
Ethnicity	white	Maghreb (northwest Africa)	Arab	Arab	Arab
Sex	female	male	female	male	male
Consanguinity	-	+	+	+	+
Hypotonia	+	+	-	+	+
Past developmental delay (motor milestones)	+	+	+	+	+
Current intellectual disability	+	+	+	+	+
Speech delay	+	+	+	+	+
Epilepsy	+	+	+	+	+
Cerebellar dysplasia/atrophy	+	+	+	+	+
Other	Scoliosis	N/A	N/A	Scoliosis	N/A

+ = evidence of certain symptoms, - = absence of certain symptoms. N/A = not applicable or not measured.

She remains non-verbal and functions at a 14-month-old toddler level (Table 1).

Individual 2 is the youngest of three children and is a 13-year-old male. His parents are first cousins. It was noted soon after his birth that he was hypotonic. He then presented with a global psychomotor development delay, sitting at 9 months and walking at 34 months. He has dysmorphic features that include a large forehead with high implanted hair, long fingers and toes, and very marked hyperlaxity. He now has intellectual disability, severe speech delay (only two syllables), stereotypic movements, and epilepsy that started when he was 7 years old (Table 1). In addition, at birth, he had a normal occipitofrontal head circumference (OFC) at 37 cm (+0.7 SD), but at the age of 11 years and 2 months, he had an OFC of 56.5 cm (+2.2 SD), a height of 137 cm (−1 SD), and a weight of 39 kg (+0.2 SD). At the age of 5 years and 7 months, he had a brain MRI that showed dilation of the Virchow-Robin spaces and mild atrophy of the superior vermis, which indicates severe cerebellar atrophy.

The parents in Family 3 are first cousins with five living children, one deceased child, and four miscarriages (Figure 1A). Two affected children are alive whereas one affected child is deceased. The other three living children are healthy. Individual 3.1 was a female with developmental delay, intellectual disability, speech delay, and epilepsy. She had generalized hypotonia with poor deep tendon reflexes, walked at the age of 2 years and 6 months with milestone regression at age 3, and subsequently lost her acquired milestones and died at the age of 11. Her epilepsy started at age 7 as myoclonic jerk and progressed to generalized clonic with multiple seizure-type EEG multispike waves. The cause of death is related to her severe global developmental delay and seizures with secondary recurrent aspiration pneumonitis and chronic lung disease. Her height was 123 cm (25^{th} percentile), her weight was 21kg (10^{th} percentile), and her head circumference was 48 cm at 8 years old (15^{th} percentile). Individuals 3.2 and 3.3 are 15- and 13-year-old males, respectively, with hypotonia, a history of developmental delay, current intellectual disability, speech delay, and epilepsy. Individual 3.2 was able to sit at 1 year of age and walked at 5 years of age, but he walked with an unsteady gait. His head circumference was 48 cm (50^{th} percentile) at 18 months, and at age 15, his height was 165 cm (25^{th} percentile) and weight was 40kg (4^{th} percentile). For individual 3.3, at age 7, his head circumference was 50.5 cm at (15^{th} percentile). At age 13, his height was 143 cm (5^{th} percentile) and weight was 35kg (5^{th} percentile). All three affected siblings had severe speech delay and were able to say only a few syllables. All three affected children had seizures, and for two of them, the seizures became controlled without medication. Individuals 3.1 and 3.3 did not have facial dysmorphism, but Individual 3.2 had subtle dysmorphic features such as tall face and mild hypertelorism. Abnormal brain MRIs showed cerebellar dysplasia and/or atrophy for the three children. Individual 3.1 had more severe abnormalities including abnormal cerebellar vermis and fourth ventricle, suggestive of a Dandy-Walker malformation.

The affected individuals have normal complete blood counts and do not show an increased susceptibility to infection, clinical immune dysfunction, exercise intolerance, fatigue, cramps, or pain.

Variants in OXR1 Are Bi-Allelic Severe LoF Mutations

Data curated by MARRVEL[46] indicate that *OXR1* is moderately to strongly intolerant of LoF variants. The gnomAD pLI score (probability of LoF intolerance)[47] of *OXR1* is 0.84 and the observed-to-expected (o/e) ratio of LoF variants is 0.19. However, heterozygous small deletions and duplications within *OXR1* exist in normal populations,

as reported in the Database of Genomic Variants.[48] This suggests that small heterozygous deletions and duplications within *OXR1* are well tolerated.

Each of the five affected individuals was found to carry bi-allelic variants in *OXR1,* and the pedigrees shown in Figure 1A document an autosomal-recessive mode of inheritance. Four variants were identified: a canonical splice donor site (+1), a canonical splice acceptor (SA) site (−1), a nonsense variant, and a frameshift (Table S2). Sanger sequencing of the fibroblasts of Individuals 2, 3.2, and 3.4 are shown in Figure S1. The four variants found in the three families are not found in gnomAD[47] and are therefore rare. These variants are predicted to be LoF and are predicted by *in silico* pathogenicity algorithms including CADD[49] and scSNV-splicing[50] to be pathogenic. The corresponding locations of the four variants are mapped onto the OXR1 protein structure (RefSeq NM_018002.3, NP_060472.2) in Figure 1C, and Table S3 lists details for each variant. *OXR1* has six validated RefSeq transcripts (Figure 1D) and RefSeq NM_018002.3 is the longest transcript that is expressed in the central nervous system (CNS). All four of the variants found in affected individuals are mapped onto the transcripts that are expressed in the CNS. Only three of the six transcripts (RefSeq NM_018002.3, NM_001198532.1, and NM_181354.4) are expressed in the CNS (as reported by GTEx; details listed in Table S3).[51]

Individual 1 is compound heterozygous for NM_018002.3:c.2082+1G>T and NM_018002.3:c.1100C>G (p.Ser367*), Individual 2 is homozygous for NM_018002.3:c.1324delA (p.Ser442Valfs*2), and Individuals 3.1, 3.2, and 3.3 were found to be homozygous for NM_018002.3:c.2236-1G>C. To determine if OXR1 is produced in these individuals, we performed immunoblots of the fibroblasts from Individuals 2 and 3.2 and showed that there are no detectable OXR1 proteins present by using two unique antibodies reported to recognize an epitope between residues 175 and 225 and an epitope between residues 267 and 359, respectively (Figure 1E, epitopes mapped to protein structure on Figure 1C). Although these epitopes are present in four of the six OXR1 isoforms, they are absent from two shorter isoforms. Therefore, levels of the two smaller isoforms, which only contain the TLDc domain (corresponding to RefSeq NM_001198535.1 and RefSeq NM_001198534.1), cannot be monitored. It is notable these two isoforms are expressed at very low or undetectable levels in the CNS (Table S3).[51] One of these isoforms, RefSeq NM_001198535.1, is expressed in testes, adrenal gland, peripheral nervous system, and salivary gland, while the other isoform, RefSeq NM_001198534.1, is not detectable or is barely detectable in all tissues.[51] These data indicate that the variants observed for 4/5 of the affected individuals correspond to LoF mutations for CNS-specific isoforms of the protein.

Loss of mustard, the Fly Homolog of OXR1, Is Lethal and Can Be Rescued by Human OXR1 and NCOA7 cDNAs

To assess the consequences of the loss of OXR1 in a model organism, we turned to *Drosophila*. The fly gene *mustard (mtd)* is predicted by 10/16 homology prediction algorithms to be the ortholog of *OXR1*.[52] Overall, *OXR1* and *mtd* are 42% similar and 29% identical, and the TLDc domain exhibits 54% identity (Figure S2). While the LysM domain is conserved in flies as well, the GRAM domain is not. First named as *l(3)82Fd*, null *mtd* mutants (*mtd*1) were found to be pupal lethal, and the pharate (emerging) adults failed to eclose of their pupal case.[53] The only other studies on the fly gene *mtd* found that it interacts genetically with *Relish,* the fly NF-κB homolog, in the innate immune system to promote survival during *Vibrio cholerae* infection.[13,14]

To test whether human *OXR1* can functionally replace the loss of *mtd*, we generated a *mtd* mutant by replacing the $Mi\{MIC\}mtd^{MI02920}$ (Minos-mediated integration cassette) with a GAL4 gene cassette.[54,55] We found that $Mi\{MIC\}mtd^{MI02920}$ does not affect *mtd* gene function because it is inserted into an intron in the wrong orientation for the SA to be effective (Figure 2A).[56] Hence, the flies were homozygous viable and healthy. Using recombinase-mediated cassette exchange (RMCE) relying on the presence of the flanking ΦC31 attP sites, we replaced the cassette with an attB-SA-T2A-GAL4-polyA-attB cassette (Figure 2A).[54,57] The SA-T2A-GAL4-polyA insertion should truncate transcription and arrest translation at the T2A site. However, translation was reinitiated to produce the GAL4 protein. This allele, referred to as *mtd-T2A-GAL4* (or *mtd-t2a-g4)* throughout, behaved genetically as a null allele, causing homozygous lethality and a failure to complement a deficiency that encompasses *mtd* (Table S4).

Homozygous (*mtd-T2A-GAL4/mtd-T2A-GAL4)* and trans-heterozygous (*mtd-T2A-GAL4/Df(3R)3-4)* mutant flies were pupal lethal, some failed to eclose properly, and a few escaped as adults with crumpled wings and died within one week (Figure 2B and 2C). To prevent the contribution of off-target mutations in the genetic background of the observed phenotypes, subsequent experiments used *mtd-T2A-GAL4/ Df(3R)3-4* flies. About 15% of the *mtd-T2A-GAL4/ Df(3R)3-4* flies eclosed as adults, escaping pupal lethality; however, all of these flies died within a few days. Pupal lethality of the *mtd* mutants could be fully rescued with the expression of an 80kb fly genomic P[acman] BAC clone (CH321-04E08,[59] Figure 2A) that covers the *mtd* locus[58] or the fly *mtd-RH* isoform cDNA (TLDc domain only). Therefore, the *mtd-T2A-GAL4/ Df(3R)3-4* phenotype is caused by the loss of the *mtd* locus (Figure 2D, Genomic Rescue Construct). Interestingly, the *mtd-T2A-GAL4/ Df(3R)3-4* lethality could also be fully rescued by a short form of the human *OXR1* cDNA that only contained the TLDc domain when driven by *mtd-T2A-GAL4* (Figure 2D, UAS-OXR1.HA). Hence, the human TLDc domain is sufficient to functionally compensate for the loss of *mtd*. Significantly, the human Nuclear Receptor

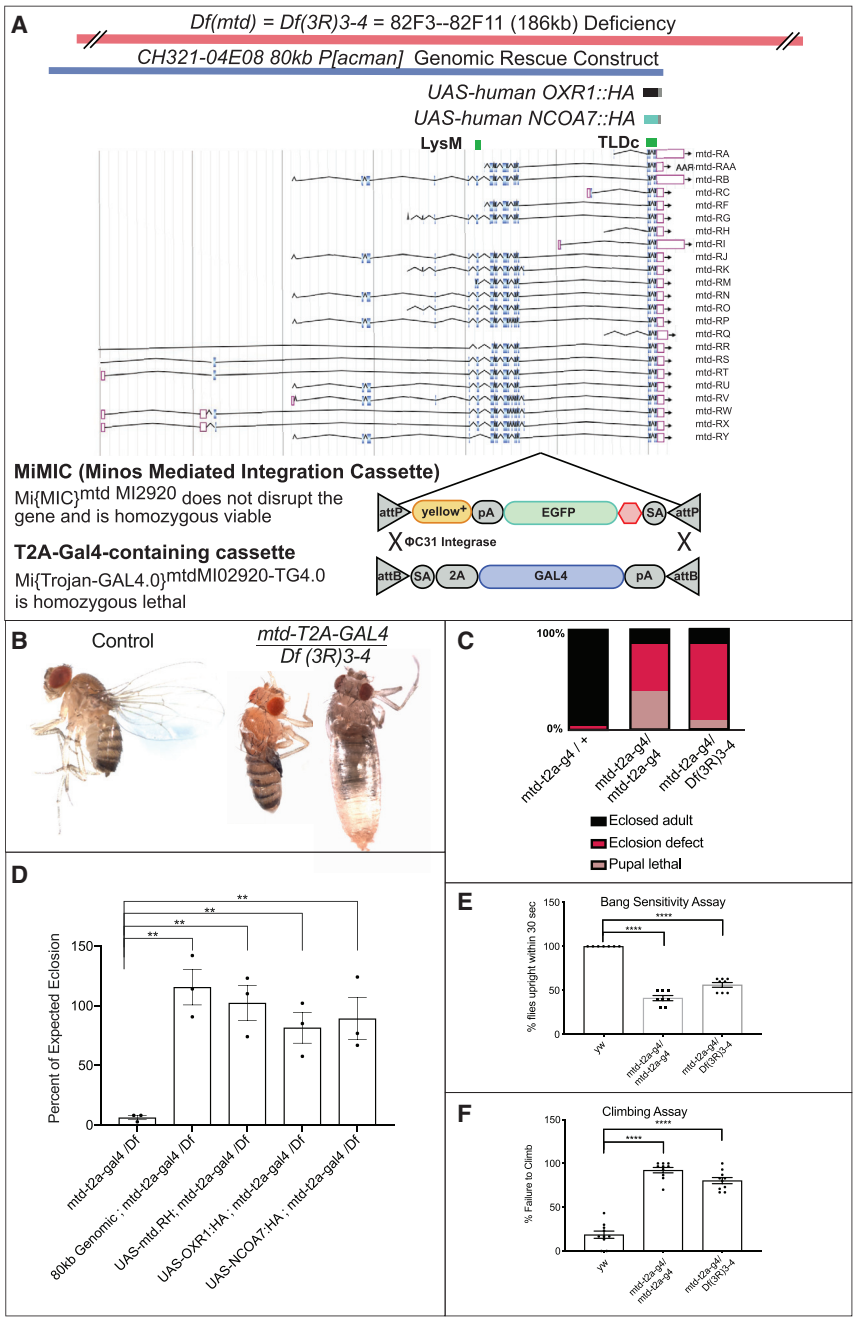

Figure 2. Loss-of-Function Alleles of *mtd* Are Lethal and Can Be Rescued by a Short Form of Human *OXR1*

(A) *mtd* fly gene structure and *mtd*-SA-T2A-Gal4-polyA allele. Twenty-three isoforms are annotated in FlyBase.[58] A Minos-mediated integration cassette (MiMIC) inserted into an intron provided a landing site for the SA-T2A-Gal4-polyA-containing cassette. Recombinase-mediated cassette exchange (RMCE) was performed with PhiC31 integrase to exchange the cassettes to generate Mi{Trojan-GAL4.0}mtd$^{MI02920\text{-}TG4.0}$ (mtd-T2A-Gal4). (pA, poly(A) signal; SA, splice-acceptor; 2A, viral T2A peptide.)

(B) The *Mi{Trojan-GAL4.0}mtd*$^{MI02920\text{-}TG4.0}$ */ Df(3R)3-4* (abbreviated *mtd-T2A-Gal4 / Df(3R)3-4*) flies mostly die as pupae, and some escapers fail to eclose. Those that did escape their pupa display wrinkled wings.

(C) Quantification of phenotypes shown in (B). Progeny from three independent crosses were counted. Escapers that reach adulthood die within the first week of life.

(D) *mtd* mutant phenotypes (*mtd-T2A-Gal4 / Df*) can be fully rescued by reintroducing 80kb fly genomic construct (CH321-04E08), fly mtd-RH cDNA, human OXR1.HA cDNA, or human NCOA7.HA cDNA. Each data point is an independent cross with at least 100 progeny. Percent of expected eclosion is calculated based on the number of observed over expected flies with the genotype on the x axis. The expected number of flies is calculated based on Mendelian ratios multiplied by the total number flies and/or progeny. A one-way ANOVA statistical test was conducted, and the p value is <0.01.

(E) Bang sensitivity is measured by quantifying the percentage of flies able to return to an upright position after 10 s of vigorous shaking on a vortex instrument. 10 flies per data point with at least 10 data points per group were tested. One-way ANOVA statistical test was conducted and the p value is < 0.0001.

(F) Climbing is measured as the percentage of flies able to climb 15 cm within 20 s. Each data point is the average of three trials with 10 flies. A one-way ANOVA statistical test was conducted, and the p value is <0.0001.

For (D), (E), and (F), two-tailed Student's t tests were conducted for data analysis. ns indicates p value >0.05, * indicates p value ≤ 0.05, ** indicates p value ≤ 0.01, *** indicates p value ≤ 0.001, **** indicates p value ≤ 0.0001. Error bars represent the standard error of the mean.

Coactivator 7 (*NCOA7*) cDNA (HGNC: 21081, RefSeq NP_001186548) (another human homolog of *mtd* containing the TLDc domain) can also rescue the lethality (Figure 2D). Flies with all four genotypes capable of rescuing *mtd* mutant lethality (*80kb genomic, UAS-mtd-RH, UAS-OXR1.HA, and UAS-NCOA7.HA* with *mtd-T2A-GAL4/ Df(3R)3-4*) also have normal wings, have no eclosion defects, and are able to reproduce.

The *mtd* mutant escaper flies were tested for bang sensitivity and climbing ability (Figure 2E and 2F) to assess their susceptibility to seizures and neurological and muscular function.[60,61] Since *mtd* mutants are mostly pupal lethal, we expected these adult escapers to be very unhealthy and to have obvious defects. Indeed, we found that the *mtd* mutants were bang sensitive and were not able to recover from a 10-second vortex (strong shaking); whereas control flies immediately returned to their upright position (Figure 2E). Consistent with lethality assays (Figure 2C), we found that homozygous (*mtd-T2A-GAL4/mtd-T2A-GAL4*) flies have a more severe

phenotype than do trans-heterozygous (*mtd-T2A-GAL4/Df(3R)3-4)* flies.

mtd mutant escaper flies also have climbing defects. In general, flies display negative geotaxis when knocked down and should climb upward naturally. Our one- to two-day-old *mtd* mutants either remained at the bottom of the vial or climbed very slowly compared to controls (Figure 2F). 19% of controls failed to climb while 92% of homozygous flies and 80% of trans-heterozygous flies failed to climb. In summary, *mtd* mutant flies are slow and uncoordinated, and this suggests either a neurological or muscular defect. However, in these young adults, histological sections of the adult brain and thorax muscles stained with hematoxylin and eosin (H&E) revealed no obvious defects when compared to controls (Figure S3).

mtd Is Broadly Expressed in the Fly CNS

To determine the cells that express *mtd,* we used the GAL4 insertion to drive a membrane-bound GFP (UAS-CD8::GFP). *mtd* is expressed in the optic lobe, mushroom bodies (memory center), and olfactory bulb of the adult fly brain, as well as in a few other neurons (Figure S4A). *mtd* is also expressed in the mushroom body and ventral nerve cord of the third instar larval brain (Figure S4B). Although it is broadly expressed, *mtd* expression is not ubiquitous in the nervous system (Figure S4A; dark areas between the visual system and the central neuropil). Although the T2A-GAL4 insertion behaves genetically as a null allele, note that five of the 23 isoforms of *mtd* are not tagged.

To determine the subcellular localization of mtd, the *mtd-T2A-GAL4* allele was used to drive human OXR1 tagged with HA (UAS-OXR1.HA), which rescues the lethality associated with the loss of *mtd*. When the adult fly brain is co-stained for anti-HA and anti-Elav, a pan-neuronal nuclear marker, these proteins co-localize in some cells, notably the nuclei of lamina neurons (Figure S4C, white arrowheads: white cells near the lamina).[62] OXR1.HA is also present in the axons, including in the lamina neurons, the dendritic projections of the lamina neurons (Figure S4D inset), and the synapses of these cells in the medulla. The magnified image in Figure S4D shows that *mtd*-expressing cells are surrounded by photoreceptors labeled by Chaoptin staining,[63] indicating that the cells that express *mtd* are L1/L2 lamina neurons (Figure S4D).

In the retina, there is only a single photoreceptor in each ommatidium that expresses *mtd* (Figures S4C). Figure 3E shows that ~70% of the *mtd*-expressing cells are marked by the R7 marker, Prospero, suggesting that *mtd* is expressed in the Rh4-expressing R7 cells (Figures S4C and S4E).[64] Interestingly, at an earlier developmental stage in the pupa (50% of pupal development), *mtd* is much more broadly expressed and is likely present in all photoreceptors (Figure S5). Hence, *mtd* is dynamically expressed during development.

Loss of mtd in Neurons Leads to Abnormal Autolysosome, Autophagosome, and/or Endolysosome Accumulation and Early Death

In order to study the neuronal phenotypes associated with *mtd,* we turned to neuronal-specific knockdown of *mtd* because *mtd* mutants are lethal at eclosion or are very short lived (Figures 2B and 2C). To assess whether RNAi knockdown replicates the *mtd* LoF phenotype, we drove the expression of five RNAis ubiquitously targeting *mtd* with *Actin-GAL4*. Three out of five RNAi lines replicate the pupal lethal eclosion defect phenotypes observed in the strong LoF mutants (Figure S6). Two of these RNAis targeted all *mtd* isoforms, whereas one targeted 18 isoforms (Figure S6). The two RNAi lines that did not replicate the phenotypes targeted 15 out of 23 isoforms of *mtd,* missing the RAA, RF, and RY isoforms that were targeted by the lethal RNAis.

Flies that expressed *mtd* RNAis in neurons, using either *elav-GAL4* or another neuronal driver, *nSyb-GAL4*,[66] die between day 10 and 15, whereas controls lived for about three months (Figure 3A). To check for specificity of RNAi (HMS01666), we overexpressed UAS-human short-form *OXR1* cDNA in the *mtd* neuronal knockdown (*elav > mtd RNAi)* background and observed a significant increase in lifespan (Figure S6C). Histological examination of *elav>mtd* RNAi fly brains using H&E staining at day 9 showed massive neuronal loss and vacuolization (Figure 3B). These data indicate that the neuronal expression of *mtd* is required for the survival of neurons. However, glial knockdown using *repo-GAL4* and muscle knockdown using *C57-GAL4* did not result in any obvious phenotypes.

To assess *mtd*'s role in neurons, we performed TEM on the retinae of *mtd* neuronal knockdown flies. Only a subset of R7 photoreceptors displayed aberrant morphological features, and the other photoreceptors and pigment glia appeared normal at days 5 and 8 (Figure 3C and D). Numerous R7 photoreceptors displayed highly aberrant shapes and dark cytoplasm typical of unhealthy photoreceptors. These photoreceptors also accumulated numerous autophagosome structures with abnormal undigested contents (Figure 3E). Typically, we observe 0–1 autophagosomes in wild-type R7 photoreceptors, whereas in *mtd* RNAi knockdowns, we observed an average of 4–6 autophagosome per section (Figure 3E).

To confirm the presence of aberrant lysosomal structures (autolysosomes, lysosomes, and endolysosomes) throughout the *elav>mtd* RNAi fly brains, we used AO dye to stain for lysosomes. AO dye is protonated at acidic pH and trapped in acidic vesicular organelles.[39] Red fluorescence of 579–620 nm emitted from AO with excitation at 561 nm is used to detect cellular autophagic activity.[39] Figure S7A shows representative images of day 3 *elav>luciferase* RNAi and elav>*mtd* RNAi flies. There is a significant increase of AO signal in *elav>mtd* RNAi flies when compared to *elav>luciferase* RNAi on both day 3 and 6 (note that these flies only live 10 days). The presence

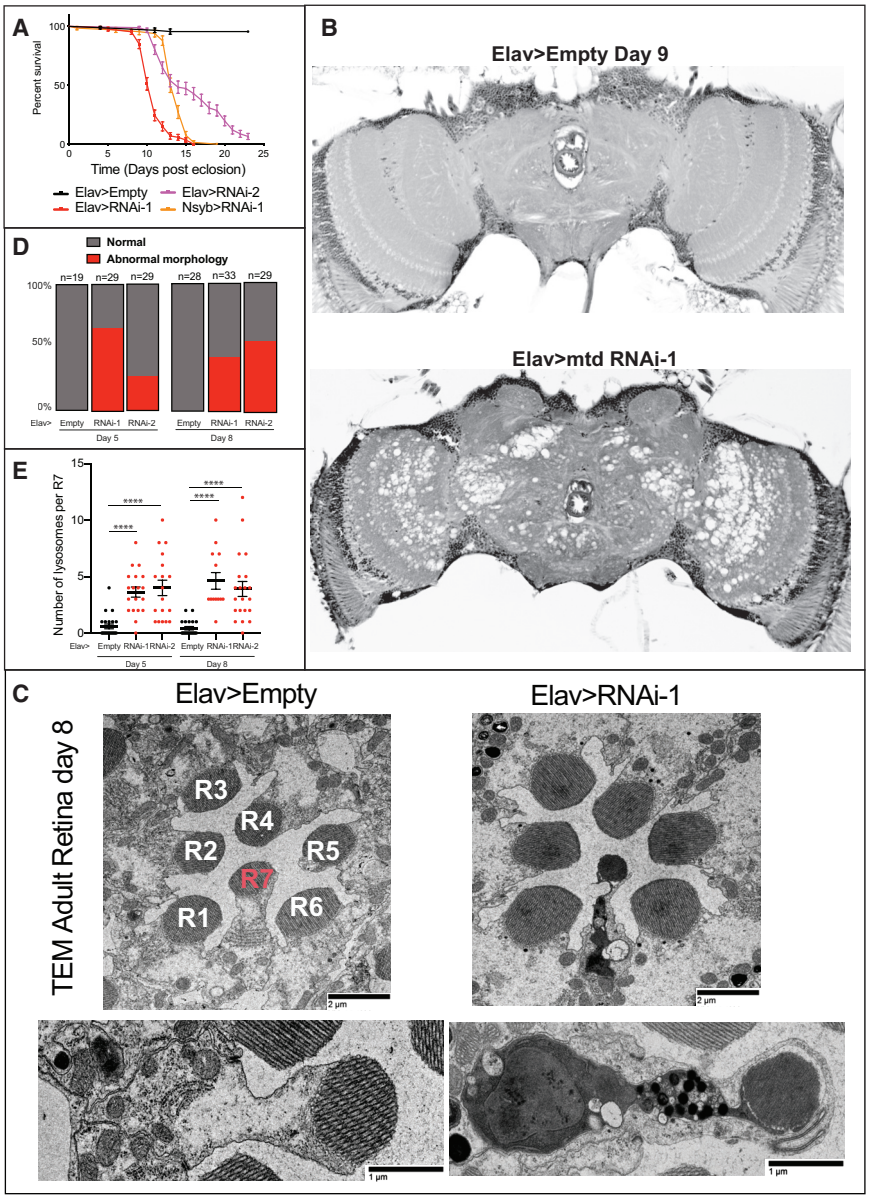

Figure 3. Neuronal Knockdown of *mustard* Leads to Selective R7 Defects and Cell Loss

(A) The lifespan of flies that express two different RNAis against *mtd*. The neuronal drivers used are elav-GAL4 and Nsyb-GAL4. The RNAi lines used are RNAi-1 (HMS01666) and RNAi-2 (GL00665).[65] n > 100 per group from three independent fly crosses. Log-rank (Mantel-Cox) and Gehan-Breslow-Wilcoxon tests were conducted for each experimental group compared to controls (Elav > Empty) and the p values are <0.0001 for all three with both tests. The error bars represent standard errors.

(B) Adult fly heads at day 9 were sectioned and stained with hematoxylin and eosin (H&E). Flies with neuronal knockdown of *mustard* exhibit severe vacuolization. At least three biological replicates were examined, and representative images are shown.

(C) Transmission electron microscopy (TEM) of the retina of Elav > empty or Elav > *mtd* RNAi adult fly heads at days 5 and 8. Photoreceptors are labeled on the left, and R7 is labeled is red. The images on the bottom show details of Elav > empty or Elav > *mtd* RNAi R7 photoreceptors. The representative images shown are consistent with results from three biological replicates.

(D) Quantification of the percentage of ommatidia with abnormal R7 cells. At least three biological replicates per group were quantified.

(E) Abnormal autophagosomes in R7 photoreceptors were quantified, and an increased number of autophagosomes were found in neuronal *mtd* knockdown conditions. At least 14 R7 photoreceptors per genotype were quantified for each group. Three biological replicates per group were processed in parallel with the same conditions and imaging settings. Two-tailed Student's t tests were conducted for data analysis. **** indicates p value ≤ 0.0001. A one-way ANOVA statistical test was conducted, and the p value is <0.0001.

of an increased number of aberrant lysosomal structures at day 3 which progresses to a more severe elevation at day 6 argues that lysosomal accumulation is a likely driver of pathogenesis. These data indicate an abnormal storage of lysosomal substrates, a defect that is often observed in lysosomal storage diseases.[67,68]

mtd Mutants Exhibit Low Levels of Oxidative Stress

OXR1 has previously been implicated in oxidative stress resistance. Human HeLa cells treated with siRNA against *OXR1* are more susceptible to H_2O_2-induced oxidative stress leading to reduced cell viability.[9] Likewise, cerebellar granule cells derived from mice that lack *Oxr1* also display a subtle increase in apoptosis when exposed to H_2O_2 compared to controls.[1] Finally, it has also been reported that the *lmd-3* mutant *C. elegans* are shorter lived when exposed to H_2O_2. However, 70% of the control animals died in a 2 h span versus 95% for the mutants.[11] In summary, these assays show that loss of *OXR1* or its homologs have subtle effects on cells or organisms when exposed to high levels of oxidative stress or other stressors like heat.[1,9,11]

To test for sensitivity to oxidative stress under *OXR1*-deficient conditions, we induced oxidative stress in flies by feeding neuronal *mtd*-deficient flies either H_2O_2 (5% and 15%) or rotenone (100μM) and measured lifespan (Figure 4A). Survival of control flies shown in red in Figure 4A is reduced after 35 days when they are fed rotenone (purple), showing that the concentration of 100μM rotenone induced a mild reduction in lifespan. In contrast,

flies in which we knock down *mtd* with RNAi (*elav>mtd* RNAi; blue) had a very severely reduced lifespan when compared to control flies (*elav>luciferase* RNAi; red); this result is consistent with the data shown in Figure 3A. When the flies in which we knock down *mtd* with RNAi are fed rotenone (green), their lifespan is mildly reduced, but this reduction in lifespan is statistically significant. These data argue that the two treatments have an additive effect. Treatment of the control flies (*elav>luciferase* RNAi) with 5% or 15% of H_2O_2 was so toxic that their lifespan was reduced to 5 and 3 days (gray and black), respectively. However, flies in which *mtd* is reduced with RNAi (*elav>mtd* RNAi) were not more susceptible to oxidative stress at 5% or 15% (orange and brown) than were the control flies. Hence, oxidative stress with H_2O_2 does not exacerbate reduced survival, but rotenone causes a mild additive effect. In summary, these data are consistent with previously published data, but they argue that loss of OXR1 leads to cells or animals that are unhealthy and are somewhat more sensitive to stressors.

To test for sensitivity to oxidative stress in affected human fibroblasts, we treated the cells with 500μM H_2O_2 for 4 h; this concentration has previously been reported to reduce viability and induce apoptosis in healthy cells (Figure 4B). After 4 h, we added PI to mark apoptotic cells and Hoechst dye to label the nuclei. The cells were washed and imaged live, and cells marked with PI were counted. The control cells (CTRL1 and Individual 3.4) exhibited a slightly higher average number of dying cells than did the fibroblasts derived from probands (Individuals 3.2 and 2). However, statistical significance was not attained in all pairwise comparisons. This suggests that *OXR1*-deficient human fibroblasts are not more sensitive to oxidative stress than are control cells.

Yang et al., 2014[9] previously showed that *OXR1*-depleted HeLa cells accumulate significantly more mitochondrial DNA (mtDNA) mutations after 1 h of exposure to 0.75mM H_2O_2 compared to control cells.[9] However, when we conducted long-range sequencing of the mtDNA of fibroblasts from proband Individual 2 with or without 1 h of 0.75mM H_2O_2 treatment, we found no increase in mutation rate and no extra deletions or insertions (Figures S8). These data show that H_2O_2 does not induce more mitochondrial DNA damage in *OXR1*-deficient human fibroblasts.

Given that the phenotypes in the fly *mtd* mutants are severe in the absence of oxidative stress or other obvious environmental challenges, we assessed the native levels of oxidative stress in the fly *mtd* mutants in the absence of obvious environmental challenges. We used *mtd-T2A-GAL4* to drive four different redox probes that measured E_{GSH} (glutathione redox potential) in the cytosol (UAS-cyto-Grx1-roGFP2) or in the mitochondrial matrix (UAS-mito-roGFP2-Grx1). We also used a cytosolic (UAS-cyto-roGFP2-Orp1) and mitochondrial matrix probe (UAS-mito-roGFP2-Orp1) to assess differences in H_2O_2 levels.[32] The oxidoreductase (Grx1)-based probe specifically and reversibly reports roGFP2 oxidation by glutathione disulfide (GSSG) and the peroxidase (Orp1)-based probe specifically and reversibly reports roGFP2 oxidation by H_2O_2.[32] To establish the full range of oxidation and reduction, fly brains were treated with the oxidant diamide (DA) and the reductant dithiothreitol (DTT) to serve as standards (top of Figure 4C). Figure 4C from left to right compares four redox probes in either *mtd-T2A-GAL4/+* or *mtd-T2A-GAL4/Df(3R)3-4* adult fly brains that are 2–3 days old. The mitochondrial probes showed no obvious difference in E_{GSH} and even a subtle decrease in H_2O_2; these results suggest that *mtd* mutant mitochondria are not affected by oxidative stress. However, we observed a mild elevation of E_{GSH} and H_2O_2 in the cytoplasm, and this indicates a mild oxidative stress in the cytoplasm of the *mtd* mutants (Figure 4D).

Oxidative damage is often observed in mitochondria, and the enzyme aconitase is exquisitely sensitive to reactive oxygen species (ROS).[69] We have previously shown that ROS-induced neurodegeneration is only present when ROS production is very elevated and associated with a 60% decrease in aconitase activity in flies.[33] We measured aconitase enzymatic activity in *mtd* mutant adult fly heads, and we observed a 20% reduction that is not statistically significant (Figure 4E). This decrease in aconitase enzymatic activity is a measure of oxidative damage and suggests that oxidative damage is very mild.[33]

To determine if antioxidants can ameliorate the lifespan of flies in which we reduce the level of *mtd* in neurons, we fed flies a number of antioxidants, including n-acetyl cysteine (NAC),[70] Oltipraz,[71] tert-Butylhydroquinone (tBHQ),[72] and 3-H-1,2-dithiole-2-thione (D3T)[34] with DMSO (the solvent) as control (Figure 4F). Although these drugs have been shown to improve elevated-ROS-mediated phenotypes in flies, we did not observe any improvement in lifespan. Together, these data indicate that oxidative stress is unlikely to be the driver of the phenotypes that we observe in *mtd* mutants.

Aberrant Lysosomal Structures Are Observed in Fibroblasts from Affected Individuals

Since we detected an accumulation of lysosomes in *mtd*-deficient R7 photoreceptors and fly brains, we investigated whether this phenotype could also be observed in primary fibroblasts of affected individuals (Individuals 2 and 3.2). Indeed, LysoTracker staining, which stains partially or fully acidified lysosomes,[73,74] revealed a significant increase in the number of lysosomes in the fibroblasts of affected individuals (Figure 5A and 5B).

To determine the ultrastructure of these acid compartments, we performed TEM. In comparison to the LysoTracker experiments, the TEM of the fibroblasts of Individual 2 revealed very elevated numbers of highly aberrant compartments filled with membranous content typical of dysfunctional lysosomes.[75] Although for Individual 3.2 the increase in these compartments was not statistically

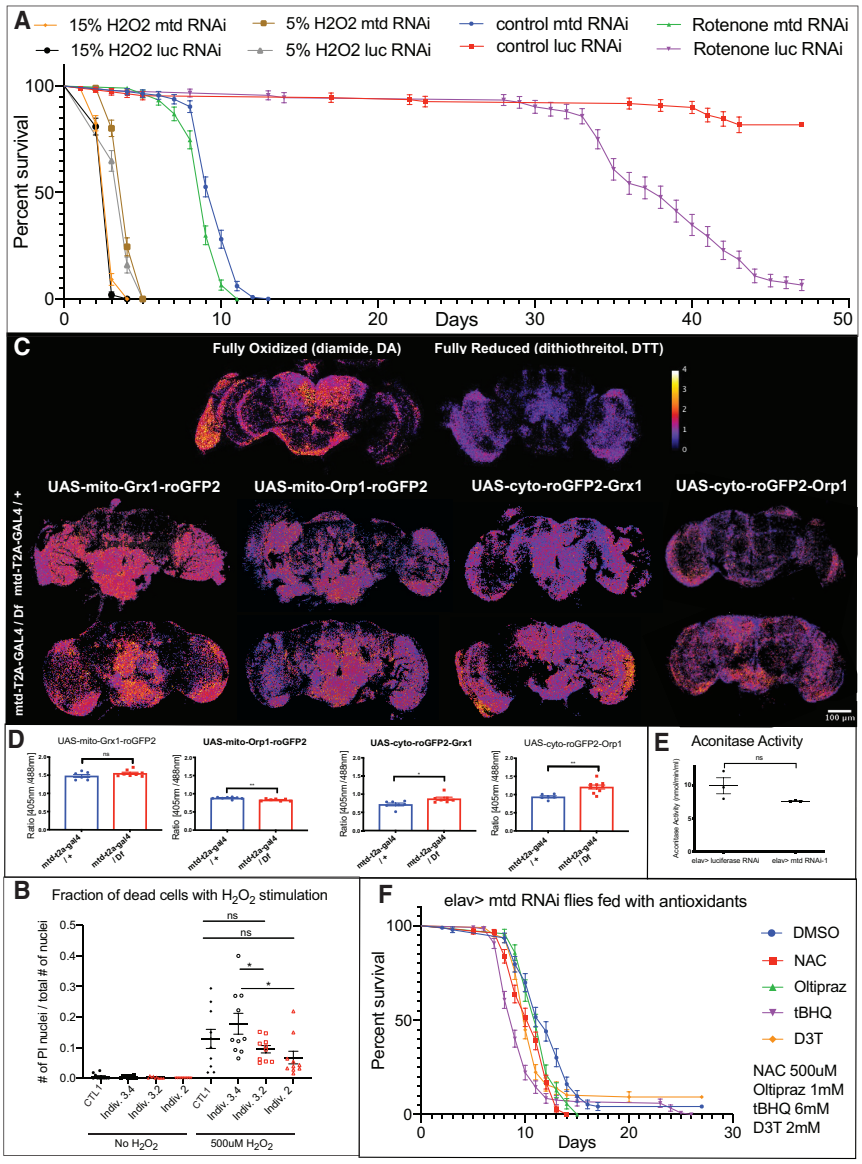

Figure 4. *mtd* Mutant Brains Show Mild Elevation of Oxidative Stress and Antioxidant Feeding Does Not Increase Lifespan of Neuronal *mtd* Knockdown Flies

(A) Elav (neuronal) > *mtd* RNAi knockdown and Elav > *luciferase* RNAi (control) flies were fed with oxidants that are known to induce reactive oxidative species. Rotenone concentrations are 100μM. Each group has >100 flies from three independent crosses. The error bars represent standard errors. Log-rank (Mantel-Cox) and Gehan-Breslow-Wilcoxon tests were conducted for the survival curves. Comparing mutant (elav > *mtd* RNAi) and control (elav > *luciferase* RNAi) flies fed with normal food, the p values are <0.0001 for both tests. Comparing mutant (elav > *mtd* RNAi) and control (elav > *luciferase* RNAi) flies fed with 100μM Rotenone, the p values are <0.0001 for both tests. Comparing flies fed with 5% H_2O_2, the p values are >0.05 for both tests. Comparing flies fed with 15% H_2O_2, the p values are >0.05 for both tests. Comparing control flies fed with normal food to control flies fed with oxidants, the p values are <0.0001 for both tests. Comparing mutant flies fed with normal food to mutant flies fed with oxidants, the p values are <0.0001 for both tests. Luc, luciferase.

(B) To test the susceptibility of OXR1-deficient fibroblasts to oxidative stress, fibroblasts were treated with 500μM H_2O_2. Dead fibroblasts' nuclei are marked by propidium iodide (PI), and total number of fibroblasts are counted by number of Hoechst positive nuclei. At least three fields are quantified from each of three biological replicates for each group. The experiments were conducted under the same conditions with the same confocal microscope settings. Two-tailed Student's t tests were conducted for data analysis. ns indicates p value > 0.05, * indicates p value ≤ 0.05. Error bars represent the standard error of the mean. A one-way ANOVA statistical test was conducted and the p value is <0.0001.

(C) The top row shows wild-type whole adult fly brains that were either fully oxidized with 2mM diamide (DA) or fully reduced with 20mM dithiothreitol (DTT) (dark purple = reduced state, yellow = oxidized state). The second and third rows show 2–3 day old *mtd-T2A-GAL4 / +* and *mtd-T2A-GAL4 / Df(3R)3-4* fly brains with four different genetically encoded oxidative stress sensors. The experiments were conducted under the same conditions with the same confocal microscope settings, and representative images are shown.

(D) Quantification of 405nm to 488nm ratio of each *in vivo* encoded reportes for either control (*mtd-t2a-gal4 / +*) or mutant (*mtd-t2a-gal4 / Df(3R)3-4*). At least five flies per group were measured. Two-tailed Student's t tests were conducted for data analysis. ns indicates p value > 0.05, * indicates p value ≤ 0.05, ** indicates p value ≤ 0.01. Error bars represent the standard error of the mean.

(E) Adult head extracts from day 5 *elav > luciferase RNAi* and *elav > mtd RNAi* flies were quantified for aconitase activity. Three biological replicates were measured. Two-tailed Student's t tests were conducted for data analysis. ns indicates p value > 0.05. Error bars represent the standard error of the mean.

(F) Elav (neuronal) > *mtd* RNAi knockdown flies were fed with DMSO and four anti-oxidation drugs. Each group has > 100 flies from three independent crosses. NAC (n-acetyl cysteine); tBHQ (tert-Butylhydroquinone); D3T (3-H-1,2-dithiole-2-thione). Log-rank (Mantel-Cox) and Gehan-Breslow-Wilcoxon tests were conducted for the survival curves. Compared with DMSO (control), the Log-rank (Mantel-Cox) p values for NAC and tBHQ are <0.0001 for NAC, and the Log-rank (Mantel-Cox) p values for Oltipraz and D3T are <0.05. The Gehan-Breslow-Wilcoxon p values for NAC and tBHQ are <0.0001 for NAC, the p value for D3T is ≤0.001, and the p value for Oltipraz is >0.05. The error bars represent standard errors.

significant, the organelles were likewise highly aberrant in structure and content (Figure 5C and 5D), and these results correspond to autolysosomes, endolysosomes, or aberrant lysosomes examined in many previous TEM data analyses.

To assess whether autophagy was functioning properly, we tested the levels of p62/Ref(2)p, a scaffold protein that facilitates degradation of ubiquitinated protein aggregates and other membranous compartments by

autophagy. It is typically localized with protein aggregates that accumulate in the presence of autophagy defects.[76] We found a significant increase in Ref(2)p/p62 in fly brains, a result that suggests that autophagy is defective (Figure S9A).[68] We also measured LAMP2 levels in fibroblasts (Figure S9B). LAMP2 is a lysosome-associated membrane glycoprotein used as a marker for lysosomes. We found that there is a statistically significant increase in LAMP2 in fibroblasts from Individual 2 and Individual 3.2 compared to those from Individual 3.4 (an unaffected sibling), but not compared to an independent control (Figure S9B).

We also conducted immunostaining in human fibroblasts for RAB7A (also called Rab7) that marks late endosomes (Figure S9C). We found a mild, but statistically significant increase in Rab7 in OXR1-deficient fibroblasts of Individual 2. In summary, the cells of proband Individual 2 have a higher number of LysoTracker positive vesicles, a higher number of abnormal lysosomal structures on TEM, and a higher level of LAMP2 and Rab7. Hence, the data are highly correlative and argue that lysosomal function is impaired in Individual 2. The cells of the other proband 3.2 are consistently not as severely affected or show no difference with the cells of proband 2 in these assays.

Discussion

Our results indicate that bi-allelic truncating or splicing mutations in *OXR1* cause a severe neurological disease with a history of developmental delay, intellectual disability, hypotonia, epilepsy, and cerebellar anomalies. Loss of *mtd,* an *OXR1* ortholog, in flies can be functionally replaced with a short cDNA of *OXR1* that contains the TLDc domain. We found that *mtd* is dynamically expressed during development and is present in many but not all adult neurons and in few glial cells. Loss of *mtd* induces an expansion of aberrant lysosomes in some photoreceptors and throughout the brain. Furthermore, neuronal loss of *mtd* causes a severe neurological phenotype that leads to early death by day 10 and also to an expanded number of lysosomes as early as day 3. We also find that *OXR1*-deficient human fibroblasts are not more susceptible to oxidative stress than are controls, and no elevation of ROS is observed in flies. Hence, our data indicate that elevated ROS is unlikely to be the main driver of disease. Instead, we argue that lysosomal dysfunction is at the root of many of the observed phenotypes.

In mammals, there are two proteins, OXR1 and NCOA7, that have similar structural domains to those of *mtd*; they contain LysM, Gram, and TLDc domains. The Drosophila RNAi Screening Center (DRSC) Integrative Ortholog Prediction Tool (DIOPT) score, a measure of orthology,[52] between *mtd* and *OXR1* is 10/16, whereas the DIOPT score between *mtd* and *NCOA7* is 9/16; this suggests that the single fly *mtd* gene plays the role of both mammalian genes. A possible redundancy between NCOA7 and OXR1 is also suggested based on evolutionary arguments. Indeed, Durand et al.[77] proposed that *NCOA7* arose from the duplication of the ancestral *OXR1* gene.[77] Loss of *mtd* is homozygous lethal in flies, and loss of *Oxr1* in mice also leads to early lethality.[5] In contrast, loss of *Ncoa7* in mice is homozygous viable but associated with abnormal kidney function.[78] However, both genes seem to be able to perform the same function given that both *OXR1* and *NCOA7* human cDNAs containing only the TLDc domain can rescue *mtd* loss in flies. This includes rescue of lethality, wing defects, eclosion defects, and other features, including fertility and climbing. Hence, *OXR1* and *NCOA7* are likely to play very similar molecular functions.

Our data support the argument that loss of *mtd* does not induce a significant increase in ROS in flies. Moreover, upon induction of stress with H_2O_2, we observed little or no increase in susceptibility to oxidative stress in *mtd* flies or human *OXR1*-deficient fibroblasts. In addition, feeding flies antioxidants that had been reported to effectively suppress ROS failed to improve the lifespan of flies with reduced *mtd* in the nervous system. Hence, the increase in ROS that we observed is unlikely to be the driver of disease. Indeed, low levels of ROS have been shown to induce downstream defense mechanisms that lead to stress resistance, and these mechanisms are thought to drive lifespan extension.[79] For example, low levels of ROS production from the mitochondria extend *Drosophila* lifespan,[80] and glucose restriction causes a mild increase in ROS; this increase is associated with an extension of lifespan in *C. elegans*.[81] Given the relationship between low levels of oxidative stress and increased longevity, the severe neurological phenotypes that we observe are unlikely to be the result of oxidative stress and are probably caused by other insults.

Our data in flies support the argument that lysosomes are increased upon loss of *mtd*. Similarly, we find an increase in LysoTracker staining as well as an accumulation of aberrant lysosomal structures in human cells derived from some probands. Interestingly, there is a much larger increase in the number of abnormal autolysosomes and/or endolysosomes in fibroblasts observed through the use of TEM compared to the number of lysosomes observed through the use of LysoTracker staining. This increase is more than 20-fold for fibroblasts derived from Individual 2. This discrepancy can be most easily explained if many of the observed aberrant lysosomes are not acidified, which would result in undigested contents accumulating in the *OXR1*-deficient fibroblasts. In flies, this increase is progressive and culminates in a severe loss of neurons when *mtd* is knocked down in neurons. Moreover, in addition to the elevation of lysosomes throughout *mtd*-deficient fly brain, TEM of *mtd*-deficient fly eyes clearly shows a cell-autonomous accumulation of highly aberrant lysosomes in cells in which *mtd* is expressed. Altogether, these data argue that a defect in lysosomal function may play an important role in the pathogenesis of LoF of *OXR1*.

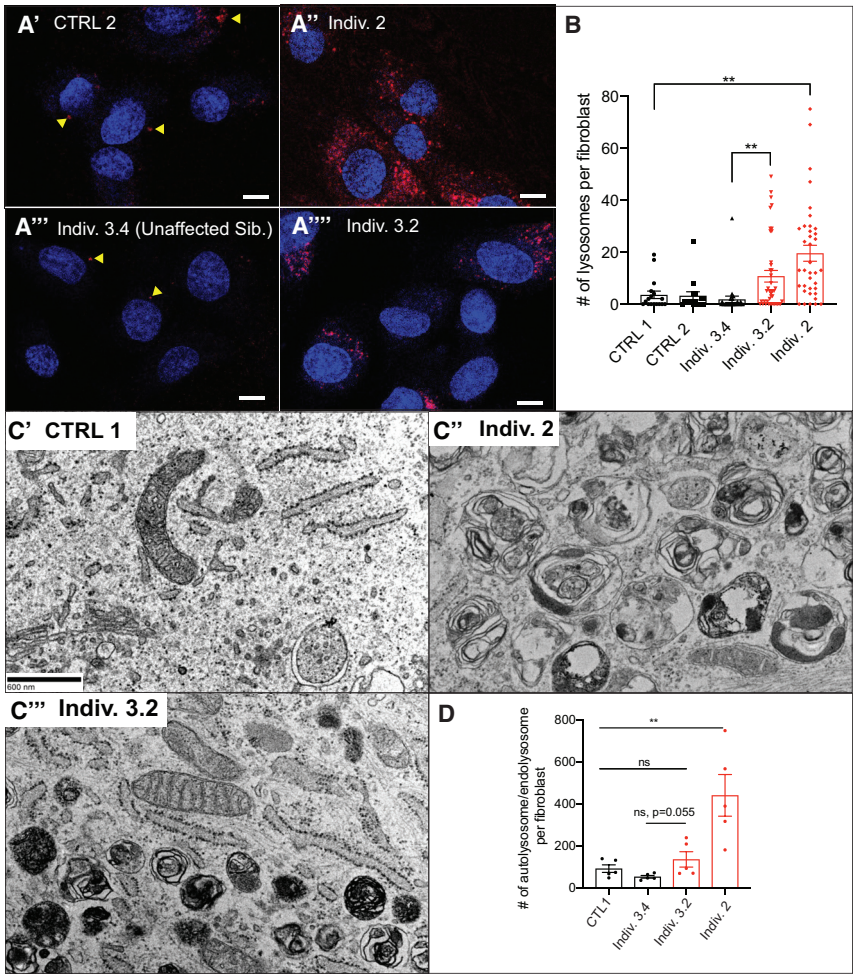

Figure 5. Human Fibroblasts that lack OXR1 Accumulate Lysosomes

(A) Human fibroblasts were stained with Lysotracker staining (red) and DAPI (blue). Yellow arrowheads indicate lysosomes. Scale bar = 10μm. The representative images shown are consistent with results from three independently performed experiments. The images were obtained from samples processed in parallel in the same experiment and acquired with identical microscopy settings.

(B) LysoTracker staining of fibroblasts was quantified by number of LysoTracker punctae in a field divided by number of nuclei. At least 10 fields from three biological replicates were counted for each group. The experiments were conducted under the same conditions with the same confocal microscope settings. A one-way ANOVA statistical test was conducted, and the p value is <0.0001. In addition, two-tailed Student t tests were conducted where ns indicates ** indicates P value ≤ 0.01. Error bars represent the standard error of the mean.

(C) Transmission electron microscopy (TEM) images of control (C') and *OXR1*-deficient (C'' and C''') fibroblasts. Scale bar = 600nm.

(D) Quantification of autolysosomes/ endolysosomes in C'-C''' and unaffected sibling from family 3 (Individual 3.4). One-way ANOVA statistical test was conducted and the p value is < 0.001. In addition, two-tailed Student t tests were conducted where ns indicates p value > 0.05, and ** indicates p value ≤ 0.01. Error bars represent the standard error of the mean.

Recently, we reported that ubiquilins and Vap proteins (VAMP-associated proteins A, B, and C) also affect lysosome acidification and cause neuronal demise.[75,82,83] However, to our knowledge, lysosomal phenotypes have not been reported in *OXR1*-deficient animals or cells. Our finding that *mtd* mutants can be rescued by *NCOA7* suggests a potential molecular mechanism for *mtd* and *OXR1*. Indeed, *NCOA7* interacts with the lysosomal Vacuolar-type H^+-ATPase (V-ATPase) subunits, and *Ncoa7* knockout mice exhibit an increase in urine pH and severely decreased abundance of V-ATPase subunits in kidney medulla cells.[78] It is interesting to note that *mtd* has been found to interact with V_1 domain subunits of the V-ATPase in proteomic studies.[84,85] Moreover, OXR1 and NCOA7 were both shown to interact with V_1 domain subunits of V-ATPase, including ATP6V1B1 and ATP6V1B2.[78,86–88] These data suggest that both OXR1 and NCOA7 have similar molecular functions. Indeed, overexpression of *NCOA7* promotes vesicle acidification, lysosomal protease activity, and degradation of lysosome contents.[78,88,89] Similarly, overexpression of Oxr1 in transgenic mice carrying $SOD1^{G93A}$, a variant that causes amyotrophic lateral sclerosis (ALS: [MIM: 105400]), extends survival and improves motor deficits.[4] Moreover, increasing Oxr1 levels in *Fus* and *Tdp-42* mice mutants, other genes that are also associated with ALS, alleviate the cellular phenotypes, including the aggregation of proteins.[3] OXR1's role in lysosomal function may underlie these beneficial effects of overexpression since, due to defects in protein homeostasis, lysosomal deficits contribute to pathology in the $SOD1^{G93A}$, FUS, TARDBP (TDP-43), and other models of ALS.[75,90–92]

Finally, a number of previously reported phenotypes associated with loss or gain of *OXR1* may be linked to autophagosomal and/or lysosomal deficits or improved lysosomal function, respectively. For example, impairing autophagy should affect mitochondrial morphology through impaired mitophagy[93] and reduce longevity as reported for mutants in which autophagy is impaired.[94,95] Moreover, overexpression of *mtd* in flies has been shown to promote tolerance to *Vibrio cholera* infections, and the toxins produced by *V. cholera* have been documented to trigger an autophagy response; this result suggests that improved lysosomal function may alleviate the infections.[12–14,96] In summary, the accumulation of aberrant lysosomal structures in mutant fly neurons and proband-derived fibroblasts support the argument that OXR1 plays a critical role in lysosomal biology.

Accession Numbers

Variants have been submitted to ClinVar, and the submission number is SUB5699650.

Supplemental Data

Supplemental Data can be found online at https://doi.org/10.1016/j.ajhg.2019.11.002.

Acknowledgments

J.W. is supported by the Eunice Kennedy Shriver National Institute of Child Health and Human Development of the National Institutes of Health (NIH) under award number F30HD094503 and the Robert and Janice McNair Foundation McNair MD/PhD Student Scholar Program. H.J.B. is supported by grant number R24OD022005 from the NIH Office of the Director, by grant number R01GM067858 from the National Institute of General Medical Sciences (NIGMS), and by the Huffington Foundation. H.J.B. is an Investigator for the Howard Hughes Medical Institute. P.M.C. is supported by clinician-scientist salary awards from the Fonds de Recherche du Québec - Santé and the Canadian Institutes of Health Research (CIHR), support from the Foundation du CHU Sainte-Justine, and a grant from the CIHR. The project was supported in part by Intellectual and Developmental Disabilities Research Center (IDDRC) grant number U54 HD083092 from the Eunice Kennedy Shriver National Institute of Child Health and Human Development. Neurovisualization Core was used for this project. We thank Anna Dennis for her contribution to this manuscript and Karen Schulze for detailed editing of this manuscript.

Declaration of Interests

W.B. and J.R. are employees of the Department of Molecular and Human Genetics at Baylor College of Medicine and Baylor Genetics Laboratories.
J.J. is an employee of GeneDx, Inc.
The other authors declare no competing interests.

Received: June 23, 2019
Accepted: November 1, 2019
Published: November 27, 2019

Web Resources

Brain RNA-seq, http://www.brainrnaseq.org/
ClinVar, https://www.ncbi.nlm.nih.gov/clinvar/
ClinVar (summary of submissions), https://www.ncbi.nlm.nih.gov/clinvar/submitters/26957
Database of Genome Variants, http://dgv.tcag.ca/
FlyBase, http://flybase.org/
Geneious, https://www.geneious.com
Genotype-Tissue Expression (GTEx) Project, https://www.gtexportal.org/home/
gnomAD, https://gnomad.broadinstitute.org
MARRVEL (Model organism Aggregated Resources for Rare Variant ExpLoration), http://marrvel.org/
OMIM, (Online Mendelian Inheritance in Man), https://www.omim.org
UniProt, https://www.uniprot.org/

References

1. Volkert, M.R., Elliott, N.A., and Housman, D.E. (2000). Functional genomics reveals a family of eukaryotic oxidation protection genes. Proc. Natl. Acad. Sci. USA *97*, 14530–14535.
2. Volkert, M.R., Wang, J.Y., and Elliott, N.A. (2008). A functional genomics approach to identify and characterize oxidation resistance genes. Methods Mol. Biol. *477*, 331–342.
3. Finelli, M.J., Liu, K.X., Wu, Y., Oliver, P.L., and Davies, K.E. (2015). Oxr1 improves pathogenic cellular features of ALS-associated FUS and TDP-43 mutations. Hum. Mol. Genet. *24*, 3529–3544.
4. Liu, K.X., Edwards, B., Lee, S., Finelli, M.J., Davies, B., Davies, K.E., and Oliver, P.L. (2015). Neuron-specific antioxidant OXR1 extends survival of a mouse model of amyotrophic lateral sclerosis. Brain *138*, 1167–1181.
5. Oliver, P.L., Finelli, M.J., Edwards, B., Bitoun, E., Butts, D.L., Becker, E.B., Cheeseman, M.T., Davies, B., and Davies, K.E. (2011). Oxr1 is essential for protection against oxidative stress-induced neurodegeneration. PLoS Genet. *7*, e1002338.
6. Natoli, R., Provis, J., Valter, K., and Stone, J. (2008). Expression and role of the early-response gene Oxr1 in the hyperoxia-challenged mouse retina. Invest. Ophthalmol. Vis. Sci. *49*, 4561–4567.
7. Elliott, N.A., and Volkert, M.R. (2004). Stress induction and mitochondrial localization of Oxr1 proteins in yeast and humans. Mol. Cell. Biol. *24*, 3180–3187.
8. Wu, Y., Davies, K.E., and Oliver, P.L. (2016). The antioxidant protein Oxr1 influences aspects of mitochondrial morphology. Free Radic. Biol. Med. *95*, 255–267.
9. Yang, M., Luna, L., Sørbø, J.G., Alseth, I., Johansen, R.F., Backe, P.H., Danbolt, N.C., Eide, L., and Bjørås, M. (2014). Human OXR1 maintains mitochondrial DNA integrity and counteracts hydrogen peroxide-induced oxidative stress by regulating antioxidant pathways involving p21. Free Radic. Biol. Med. *77*, 41–48.
10. Zhang, X., Zhang, S., Liu, X., Wang, Y., Chang, J., Zhang, X., Mackintosh, S.G., Tackett, A.J., He, Y., Lv, D., et al. (2018). Oxidation resistance 1 is a novel senolytic target. Aging Cell *17*, e12780.
11. Sanada, Y., Asai, S., Ikemoto, A., Moriwaki, T., Nakamura, N., Miyaji, M., and Zhang-Akiyama, Q.M. (2014). Oxidation resistance 1 is essential for protection against oxidative stress and participates in the regulation of aging in Caenorhabditis elegans. Free Radic. Res. *48*, 919–928.
12. Su, L.D., Zhang, Q.L., and Lu, Z. (2017). Oxidation resistance 1 (OXR1) participates in silkworm defense against bacterial infection through the JNK pathway. Insect Sci. *24*, 17–26.
13. Wang, Z., Hang, S., Purdy, A.E., and Watnick, P.I. (2013). Mutations in the IMD pathway and mustard counter Vibrio cholerae suppression of intestinal stem cell division in Drosophila. MBio *4*, e00337–e13.
14. Wang, Z., Berkey, C.D., and Watnick, P.I. (2012). The Drosophila protein mustard tailors the innate immune response activated by the immune deficiency pathway. J. Immunol. *188*, 3993–4000.
15. Li, Y., Li, W., Liu, C., Yan, M., Raman, I., Du, Y., Fang, X., Zhou, X.J., Mohan, C., and Li, Q.Z. (2014). Delivering oxidation resistance-1 (OXR1) to mouse kidney by genetic modified mesenchymal stem cells exhibited enhanced protection

against nephrotoxic serum induced renal injury and lupus nephritis. J. Stem Cell Res. Ther. *4*, 1000231.
16. Yang, M., Lin, X., Rowe, A., Rognes, T., Eide, L., and Bjørås, M. (2015). Transcriptome analysis of human OXR1 depleted cells reveals its role in regulating the p53 signaling pathway. Sci. Rep. *5*, 17409.
17. Finelli, M.J., Paramo, T., Pires, E., Ryan, B.J., Wade-Martins, R., Biggin, P.C., McCullagh, J., and Oliver, P.L. (2019). Oxidation resistance 1 modulates glycolytic pathways in the cerebellum via an interaction with glucose-6-phosphate isomerase. Mol. Neurobiol. *56*, 1558–1577.
18. Mitchell, A.L., Attwood, T.K., Babbitt, P.C., Blum, M., Bork, P., Bridge, A., Brown, S.D., Chang, H.Y., El-Gebali, S., Fraser, M.I., et al. (2019). InterPro in 2019: Improving coverage, classification and access to protein sequence annotations. Nucleic Acids Res. *47* (D1), D351–D360.
19. Letunic, I., and Bork, P. (2018). 20 years of the SMART protein domain annotation resource. Nucleic Acids Res. *46* (D1), D493–D496.
20. Blaise, M., Alsarraf, H.M., Wong, J.E., Midtgaard, S.R., Laroche, F., Schack, L., Spaink, H., Stougaard, J., and Thirup, S. (2012). Crystal structure of the TLDc domain of oxidation resistance protein 2 from zebrafish. Proteins *80*, 1694–1698.
21. Finelli, M.J., Sanchez-Pulido, L., Liu, K.X., Davies, K.E., and Oliver, P.L. (2016). The evolutionarily conserved Tre2/Bub2/Cdc16 (TBC), lysin motif (LysM), domain catalytic (TLDc) domain is neuroprotective against oxidative stress. J. Biol. Chem. *291*, 2751–2763.
22. Murphy, K.C., and Volkert, M.R. (2012). Structural/functional analysis of the human OXR1 protein: identification of exon 8 as the anti-oxidant encoding function. BMC Mol. Biol. *13*, 26.
23. Costantini, A., Valta, H., Baratang, N.V., Yap, P., Bertola, D.R., Yamamoto, G.L., Kim, C.A., Chen, J., Wierenga, K.J., Fanning, E.A., et al. (2019). Novel fibronectin mutations and expansion of the phenotype in spondylometaphyseal dysplasia with "corner fractures". Bone *121*, 163–171.
24. Thevenon, J., Duffourd, Y., Masurel-Paulet, A., Lefebvre, M., Feillet, F., El Chehadeh-Djebbar, S., St-Onge, J., Steinmetz, A., Huet, F., Chouchane, M., et al. (2016). Diagnostic odyssey in severe neurodevelopmental disorders: toward clinical whole-exome sequencing as a first-line diagnostic test. Clin. Genet. *89*, 700–707.
25. Monies, D., Abouelhoda, M., AlSayed, M., Alhassnan, Z., Alotaibi, M., Kayyali, H., Al-Owain, M., Shah, A., Rahbeeni, Z., Al-Muhaizea, M.A., et al. (2017). The landscape of genetic diseases in Saudi Arabia based on the first 1000 diagnostic panels and exomes. Hum. Genet. *136*, 921–939.
26. Sobreira, N., Schiettecatte, F., Valle, D., and Hamosh, A. (2015). GeneMatcher: A matching tool for connecting investigators with an interest in the same gene. Hum. Mutat. *36*, 928–930.
27. Villegas, J., and McPhaul, M. (2005). Establishment and culture of human skin fibroblasts. Curr. Protoc. Mol. Biol. *71*, 28.3.1–28.3.9.
28. Abramov, A.Y., Smulders-Srinivasan, T.K., Kirby, D.M., Acin-Perez, R., Enriquez, J.A., Lightowlers, R.N., Duchen, M.R., and Turnbull, D.M. (2010). Mechanism of neurodegeneration of neurons with mitochondrial DNA mutations. Brain *133*, 797–807.
29. Palculict, M.E., Zhang, V.W., Wong, L.J., and Wang, J. (2016). comprehensive mitochondrial genome analysis by massively parallel sequencing. Methods Mol. Biol. *1351*, 3–17.
30. Zhang, W., Cui, H., and Wong, L.J. (2012). Comprehensive one-step molecular analyses of mitochondrial genome by massively parallel sequencing. Clin. Chem. *58*, 1322–1331.
31. Saras, A., Wu, V.V., Brawer, H.J., and Tanouye, M.A. (2017). Investigation of seizure-susceptibility in a *Drosophila melanogaster* model of human epilepsy with optogenetic stimulation. Genetics *206*, 1739–1746.
32. Albrecht, S.C., Barata, A.G., Grosshans, J., Teleman, A.A., and Dick, T.P. (2011). In vivo mapping of hydrogen peroxide and oxidized glutathione reveals chemical and regional specificity of redox homeostasis. Cell Metab. *14*, 819–829.
33. Liu, L., Zhang, K., Sandoval, H., Yamamoto, S., Jaiswal, M., Sanz, E., Li, Z., Hui, J., Graham, B.H., Quintana, A., and Bellen, H.J. (2015). Glial lipid droplets and ROS induced by mitochondrial defects promote neurodegeneration. Cell *160*, 177–190.
34. Soriano, F.X., Léveillé, F., Papadia, S., Higgins, L.G., Varley, J., Baxter, P., Hayes, J.D., and Hardingham, G.E. (2008). Induction of sulfiredoxin expression and reduction of peroxiredoxin hyperoxidation by the neuroprotective Nrf2 activator 3H-1,2-dithiole-3-thione. J. Neurochem. *107*, 533–543.
35. Konwinski, R.R., Haddad, R., Chun, J.A., Klenow, S., Larson, S.C., Haab, B.B., and Furge, L.L. (2004). Oltipraz, 3H-1,2-dithiole-3-thione, and sulforaphane induce overlapping and protective antioxidant responses in murine microglial cells. Toxicol. Lett. *153*, 343–355.
36. Costa, A.C., Loh, S.H., and Martins, L.M. (2013). Drosophila Trap1 protects against mitochondrial dysfunction in a PINK1/parkin model of Parkinson's disease. Cell Death Dis. *4*, e467.
37. Sur, M., Dey, P., Sarkar, A., Bar, S., Banerjee, D., Bhat, S., and Mukherjee, P. (2018). Sarm1 induction and accompanying inflammatory response mediates age-dependent susceptibility to rotenone-induced neurotoxicity. Cell Death Discov. *4*, 114.
38. Blackney, M.J., Cox, R., Shepherd, D., and Parker, J.D. (2014). Cloning and expression analysis of Drosophila extracellular Cu Zn superoxide dismutase. Biosci. Rep. *34*, e00164.
39. Thomé, M.P., Filippi-Chiela, E.C., Villodre, E.S., Migliavaca, C.B., Onzi, G.R., Felipe, K.B., and Lenz, G. (2016). Ratiometric analysis of Acridine Orange staining in the study of acidic organelles and autophagy. J. Cell Sci. *129*, 4622–4632.
40. Park, Y.-J., Kim, S., Shim, H.-P., Park, J.H., Lee, G., Kim, T.-Y., Jo, M.-C., Kwon, A.-Y., Lee, M., Kwon, S.-H., et al. (2019). Mutations of the Gongpo Gene Encoding a Homolog of Mammalian Phosphatidylserine Synthases Cause Neurodegeneration in Drosophila Melanogaster (SSRN Electronic Journal). https://doi.org/10.2139/ssrn.3443687.
41. Rui, Y.N., Xu, Z., Patel, B., Chen, Z., Chen, D., Tito, A., David, G., Sun, Y., Stimming, E.F., Bellen, H.J., et al. (2015). Huntingtin functions as a scaffold for selective macroautophagy. Nat. Cell Biol. *17*, 262–275.
42. Campbell, G., Göring, H., Lin, T., Spana, E., Andersson, S., Doe, C.Q., and Tomlinson, A. (1994). RK2, a glial-specific homeodomain protein required for embryonic nerve cord condensation and viability in Drosophila. Development *120*, 2957–2966.
43. Fujita, S.C., Zipursky, S.L., Benzer, S., Ferrús, A., and Shotwell, S.L. (1982). Monoclonal antibodies against the Drosophila nervous system. Proc. Natl. Acad. Sci. USA *79*, 7929–7933.
44. Tan, K.L., Haelterman, N.A., Kwartler, C.S., Regalado, E.S., Lee, P.T., Nagarkar-Jaiswal, S., Guo, D.C., Duraine, L., Wangler, M.F., Bamshad, M.J., et al.; University of Washington Center

for Mendelian Genomics (2018). Ari-1 regulates myonuclear organization together with parkin and is associated with aortic aneurysms. Dev. Cell *45*, 226–244.e8.
45. Ugur, B., Bao, H., Stawarski, M., Duraine, L.R., Zuo, Z., Lin, Y.Q., Neely, G.G., Macleod, G.T., Chapman, E.R., and Bellen, H.J. (2017). The Krebs cycle enzyme isocitrate dehydrogenase 3A couples mitochondrial metabolism to synaptic transmission. Cell Rep. *21*, 3794–3806.
46. Wang, J., Al-Ouran, R., Hu, Y., Kim, S.Y., Wan, Y.W., Wangler, M.F., Yamamoto, S., Chao, H.T., Comjean, A., Mohr, S.E., et al.; UDN (2017). MARRVEL: Integration of Human and Model Organism Genetic Resources to Facilitate Functional Annotation of the Human Genome. Am. J. Hum. Genet. *100*, 843–853.
47. Karczewski, K.J., Francioli, L.C., Tiao, G., Cummings, B.B., Alföldi, J., Wang, Q., Collins, R.L., Laricchia, K.M., Ganna, A., Birnbaum, D.P., et al. (2019). Variation across 141,456 human exomes and genomes reveals the spectrum of loss-of-function intolerance across human protein-coding genes. bioRxiv, 531210.
48. MacDonald, J.R., Ziman, R., Yuen, R.K., Feuk, L., and Scherer, S.W. (2014). The Database of Genomic Variants: A curated collection of structural variation in the human genome. Nucleic Acids Res. *42*, D986–D992.
49. Rentzsch, P., Witten, D., Cooper, G.M., Shendure, J., and Kircher, M. (2019). CADD: Predicting the deleteriousness of variants throughout the human genome. Nucleic Acids Res. *47* (D1), D886–D894.
50. Jian, X., Boerwinkle, E., and Liu, X. (2014). In silico prediction of splice-altering single nucleotide variants in the human genome. Nucleic Acids Res. *42*, 13534–13544.
51. Carithers, L.J., and Moore, H.M. (2015). The Genotype-Tissue Expression (GTEx) Project. Biopreserv. Biobank. *13*, 307–308.
52. Hu, Y., Flockhart, I., Vinayagam, A., Bergwitz, C., Berger, B., Perrimon, N., and Mohr, S.E. (2011). An integrative approach to ortholog prediction for disease-focused and other functional studies. BMC Bioinformatics *12*, 357.
53. Stowers, R.S., Russell, S., and Garza, D. (1999). The 82F late puff contains the L82 gene, an essential member of a novel gene family. Dev. Biol. *213*, 116–130.
54. Lee, P.T., Zirin, J., Kanca, O., Lin, W.W., Schulze, K.L., Li-Kroeger, D., Tao, R., Devereaux, C., Hu, Y., Chung, V., et al. (2018). A gene-specific *T2A-GAL4* library for *Drosophila*. eLife *7*, e35574.
55. Diao, F., Ironfield, H., Luan, H., Diao, F., Shropshire, W.C., Ewer, J., Marr, E., Potter, C.J., Landgraf, M., and White, B.H. (2015). Plug-and-play genetic access to Drosophila cell types using exchangeable exon cassettes. Cell Rep. *10*, 1410–1421.
56. Nagarkar-Jaiswal, S., Lee, P.T., Campbell, M.E., Chen, K., Anguiano-Zarate, S., Gutierrez, M.C., Busby, T., Lin, W.W., He, Y., Schulze, K.L., et al. (2015). A library of MiMICs allows tagging of genes and reversible, spatial and temporal knockdown of proteins in Drosophila. eLife *4*, e05338.
57. Diao, F., and White, B.H. (2012). A novel approach for directing transgene expression in Drosophila: T2A-Gal4 in-frame fusion. Genetics *190*, 1139–1144.
58. Thurmond, J., Goodman, J.L., Strelets, V.B., Attrill, H., Gramates, L.S., Marygold, S.J., Matthews, B.B., Millburn, G., Antonazzo, G., Trovisco, V., et al.; FlyBase Consortium (2019). FlyBase 2.0: The next generation. Nucleic Acids Res. *47* (D1), D759–D765.
59. Venken, K.J., Carlson, J.W., Schulze, K.L., Pan, H., He, Y., Spokony, R., Wan, K.H., Koriabine, M., de Jong, P.J., White, K.P., et al. (2009). Versatile P[acman] BAC libraries for transgenesis studies in Drosophila melanogaster. Nat. Methods *6*, 431–434.
60. Stone, B., Burke, B., Pathakamuri, J., Coleman, J., and Kuebler, D. (2014). A low-cost method for analyzing seizure-like activity and movement in Drosophila. J. Vis. Exp. *19*, e51460.
61. Song, J., and Tanouye, M.A. (2008). From bench to drug: Human seizure modeling using Drosophila. Prog. Neurobiol. *84*, 182–191.
62. Tan, L., Zhang, K.X., Pecot, M.Y., Nagarkar-Jaiswal, S., Lee, P.T., Takemura, S.Y., McEwen, J.M., Nern, A., Xu, S., Tadros, W., et al. (2015). Ig superfamily ligand and receptor pairs expressed in synaptic partners in Drosophila. Cell *163*, 1756–1769.
63. Van Vactor, D., Jr., Krantz, D.E., Reinke, R., and Zipursky, S.L. (1988). Analysis of mutants in chaoptin, a photoreceptor cell-specific glycoprotein in Drosophila, reveals its role in cellular morphogenesis. Cell *52*, 281–290.
64. Wernet, M.F., Mazzoni, E.O., Çelik, A., Duncan, D.M., Duncan, I., and Desplan, C. (2006). Stochastic spineless expression creates the retinal mosaic for colour vision. Nature *440*, 174–180.
65. Perkins, L.A., Holderbaum, L., Tao, R., Hu, Y., Sopko, R., McCall, K., Yang-Zhou, D., Flockhart, I., Binari, R., Shim, H.-S., et al. (2015). The Transgenic RNAi Project at Harvard Medical School: Resources and validation. Genetics *201*, 843–852.
66. Broadie, K., Prokop, A., Bellen, H.J., O'Kane, C.J., Schulze, K.L., and Sweeney, S.T. (1995). Syntaxin and synaptobrevin function downstream of vesicle docking in Drosophila. Neuron *15*, 663–673.
67. Parenti, G., Andria, G., and Ballabio, A. (2015). Lysosomal storage diseases: from pathophysiology to therapy. Annu. Rev. Med. *66*, 471–486.
68. Platt, F.M., Boland, B., and van der Spoel, A.C. (2012). The cell biology of disease: lysosomal storage disorders: the cellular impact of lysosomal dysfunction. J. Cell Biol. *199*, 723–734.
69. Yan, L.J., Levine, R.L., and Sohal, R.S. (1997). Oxidative damage during aging targets mitochondrial aconitase. Proc. Natl. Acad. Sci. USA *94*, 11168–11172.
70. Bavarsad Shahripour, R., Harrigan, M.R., and Alexandrov, A.V. (2014). N-acetylcysteine (NAC) in neurological disorders: mechanisms of action and therapeutic opportunities. Brain Behav. *4*, 108–122.
71. Sykiotis, G.P., and Bohmann, D. (2008). Keap1/Nrf2 signaling regulates oxidative stress tolerance and lifespan in Drosophila. Dev. Cell *14*, 76–85.
72. Bahia, P.K., Pugh, V., Hoyland, K., Hensley, V., Rattray, M., and Williams, R.J. (2012). Neuroprotective effects of phenolic antioxidant tBHQ associate with inhibition of FoxO3a nuclear translocation and activity. J. Neurochem. *123*, 182–191.
73. Duvvuri, M., Gong, Y., Chatterji, D., and Krise, J.P. (2004). Weak base permeability characteristics influence the intracellular sequestration site in the multidrug-resistant human leukemic cell line HL-60. J. Biol. Chem. *279*, 32367–32372.
74. Mindell, J.A. (2012). Lysosomal acidification mechanisms. Annu. Rev. Physiol. *74*, 69–86.
75. Mao, D., Lin, G., Tepe, B., Zuo, Z., Tan, K.L., Senturk, M., Zhang, S., Arenkiel, B.R., Sardiello, M., and Bellen, H.J. (2019). VAMP associated proteins are required for autophagic

and lysosomal degradation by promoting a PtdIns4P-mediated endosomal pathway. Autophagy *15*, 1214–1233.
76. Pankiv, S., Clausen, T.H., Lamark, T., Brech, A., Bruun, J.A., Outzen, H., Øvervatn, A., Bjørkøy, G., and Johansen, T. (2007). p62/SQSTM1 binds directly to Atg8/LC3 to facilitate degradation of ubiquitinated protein aggregates by autophagy. J. Biol. Chem. *282*, 24131–24145.
77. Durand, M., Kolpak, A., Farrell, T., Elliott, N.A., Shao, W., Brown, M., and Volkert, M.R. (2007). The OXR domain defines a conserved family of eukaryotic oxidation resistance proteins. BMC Cell Biol. *8*, 13.
78. Merkulova, M., Păunescu, T.G., Nair, A.V., Wang, C.Y., Capen, D.E., Oliver, P.L., Breton, S., and Brown, D. (2018). Targeted deletion of the Ncoa7 gene results in incomplete distal renal tubular acidosis in mice. Am. J. Physiol. Renal Physiol. *315*, F173–F185.
79. Ristow, M., and Schmeisser, S. (2011). Extending life span by increasing oxidative stress. Free Radic. Biol. Med. *51*, 327–336.
80. Scialò, F., Sriram, A., Fernández-Ayala, D., Gubina, N., Lõhmus, M., Nelson, G., Logan, A., Cooper, H.M., Navas, P., Enríquez, J.A., et al. (2016). Mitochondrial ROS produced via reverse electron transport extend animal lifespan. Cell Metab. *23*, 725–734.
81. Schulz, T.J., Zarse, K., Voigt, A., Urban, N., Birringer, M., and Ristow, M. (2007). Glucose restriction extends Caenorhabditis elegans life span by inducing mitochondrial respiration and increasing oxidative stress. Cell Metab. *6*, 280–293.
82. Şentürk, M., Mao, D., and Bellen, H.J. (2019). Loss of proteins associated with amyotrophic lateral sclerosis affects lysosomal acidification via different routes. Autophagy *15*, 1467–1469.
83. Şentürk, M., Lin, G., Zuo, Z., Mao, D., Watson, E., Mikos, A.G., and Bellen, H.J. (2019). Ubiquilins regulate autophagic flux through mTOR signalling and lysosomal acidification. Nat. Cell Biol. *21*, 384–396.
84. Hu, Y., Vinayagam, A., Nand, A., Comjean, A., Chung, V., Hao, T., Mohr, S.E., and Perrimon, N. (2018). Molecular Interaction Search Tool (MIST): an integrated resource for mining gene and protein interaction data. Nucleic Acids Res. *46* (D1), D567–D574.
85. Guruharsha, K.G., Rual, J.F., Zhai, B., Mintseris, J., Vaidya, P., Vaidya, N., Beekman, C., Wong, C., Rhee, D.Y., Cenaj, O., et al. (2011). A protein complex network of Drosophila melanogaster. Cell *147*, 690–703.
86. Merkulova, M., Păunescu, T.G., Azroyan, A., Marshansky, V., Breton, S., and Brown, D. (2015). Mapping the H(+) (V)-ATPase interactome: identification of proteins involved in trafficking, folding, assembly and phosphorylation. Sci. Rep. *5*, 14827.
87. Huttlin, E.L., Ting, L., Bruckner, R.J., Gebreab, F., Gygi, M.P., Szpyt, J., Tam, S., Zarraga, G., Colby, G., Baltier, K., et al. (2015). The BioPlex Network: A Systematic Exploration of the Human Interactome. Cell *162*, 425–440.
88. Doyle, T., Moncorgé, O., Bonaventure, B., Pollpeter, D., Lussignol, M., Tauziet, M., Apolonia, L., Catanese, M.T., Goujon, C., and Malim, M.H. (2018). The interferon-inducible isoform of NCOA7 inhibits endosome-mediated viral entry. Nat. Microbiol. *3*, 1369–1376.
89. Yu, L., Croze, E., Yamaguchi, K.D., Tran, T., Reder, A.T., Litvak, V., and Volkert, M.R. (2015). Induction of a unique isoform of the NCOA7 oxidation resistance gene by interferon β-1b. J. Interferon Cytokine Res. *35*, 186–199.
90. Rudnick, N.D., Griffey, C.J., Guarnieri, P., Gerbino, V., Wang, X., Piersaint, J.A., Tapia, J.C., Rich, M.M., and Maniatis, T. (2017). Distinct roles for motor neuron autophagy early and late in the $SOD1^{G93A}$ mouse model of ALS. Proc. Natl. Acad. Sci. USA *114*, E8294–E8303.
91. Xie, Y., Zhou, B., Lin, M.Y., Wang, S., Foust, K.D., and Sheng, Z.H. (2015). Endolysosomal deficits augment mitochondria pathology in spinal motor neurons of asymptomatic fALS mice. Neuron *87*, 355–370.
92. Ramesh, N., and Pandey, U.B. (2017). Autophagy dysregulation in ALS: When protein aggregates get out of hand. Front. Mol. Neurosci. *10*, 263.
93. Pickles, S., Vigié, P., and Youle, R.J. (2018). Mitophagy and quality control mechanisms in mitochondrial maintenance. Curr. Biol. *28*, R170–R185.
94. Hansen, M., Rubinsztein, D.C., and Walker, D.W. (2018). Autophagy as a promoter of longevity: insights from model organisms. Nat. Rev. Mol. Cell Biol. *19*, 579–593.
95. Yoon, W.H., Sandoval, H., Nagarkar-Jaiswal, S., Jaiswal, M., Yamamoto, S., Haelterman, N.A., Putluri, N., Putluri, V., Sreekumar, A., Tos, T., et al. (2017). Loss of nardilysin, a mitochondrial co-chaperone for α-ketoglutarate dehydrogenase, promotes mTORC1 activation and neurodegeneration. Neuron *93*, 115–131.
96. Elluri, S., Enow, C., Vdovikova, S., Rompikuntal, P.K., Dongre, M., Carlsson, S., Pal, A., Uhlin, B.E., and Wai, S.N. (2014). Outer membrane vesicles mediate transport of biologically active Vibrio cholerae cytolysin (VCC) from V. cholerae strains. PLoS ONE *9*, e106731.